X89-36078

NASA Technical Memorandum 4147

Low-Speed Wind-Tunnel Study of Reaction Control-Jet Effectiveness for Hover and Transition of a STOVL Fighter Concept

Donald R. Riley, Gautam H. Shah,
and Richard E. Kuhn

DECEMBER 1989

NASA

NASA Technical Memorandum 4147

Low-Speed Wind-Tunnel Study of Reaction Control-Jet Effectiveness for Hover and Transition of a STOVL Fighter Concept

Donald R. Riley and Gautam H. Shah
Langley Research Center
Hampton, Virginia

Richard E. Kuhn
San Diego, California

National Aeronautics and
Space Administration
Office of Management
Scientific and Technical
Information Division

1989

Summary

A brief wind-tunnel study was conducted in the Langley 12-Foot Low-Speed Tunnel to determine reaction control-jet effectiveness and some associated aerodynamic characteristics of a 15-percent-scale model of the General Dynamics E-7A STOVL fighter concept applicable to hover and transition flight. Where possible, the measured data were compared with values calculated using empirical methods. Results showed a loss in control-jet effectiveness with increasing forward speed for transition conditions for the baseline roll-jet location. Smaller losses in control-jet effectiveness were measured for the nose jet and yaw jets with increasing forward speed. A smaller loss in effectiveness was obtained by several alternate roll-jet locations than by the baseline roll-jet location.

Introduction

Attitude control of vertical takeoff and landing (VTOL) and short takeoff and vertical landing (STOVL) aircraft in hovering and low-speed flight can be accomplished using reaction control jets placed at various locations on the aircraft. Unfortunately, the forces and moments generated by such control jets do not necessarily remain invariant when the aircraft is hovering in a crosswind or in transition flight. (See ref. 1.) The loss of control-jet effectiveness is similar to the lift loss induced by main jets which is a widely recognized phenomenon that has been reported at various times in the literature. (For example, see refs. 2–6.) Tests of specific configurations are usually made because of the lack of an adequate theory for computing control-jet effectiveness for the wide variety of possible control-jet locations employed in various aircraft designs. Reference 7 represents the only published data available on the loss of control-jet effectiveness. Reference 1 gives an analysis of these data.

The present paper presents the results involving reaction control jets that were obtained during a wind-tunnel investigation of a 15-percent-scale powered model of a single-engine STOVL fighter concept conducted in the Langley 12-Foot Low-Speed Tunnel. The aircraft concept is the General Dynamics E-7A advanced supersonic fighter design with an ejector-augmentor system located forward of the center of gravity in the wing root section of a large clipped delta wing and a vectorable core nozzle located aft of the center of gravity to provide the lift and balance required for short takeoff and vertical landing capability. Reaction control jets for attitude control are located in the nose, wing, and tail sections. The purpose of this paper is to report preliminary results applicable to transition flight on the effectiveness of the reaction control jets studied. In addition to the original design, several alternate locations of the roll jets were examined. For all test results, the main engine simulator was unpowered, the wing ejector diffusers were deployed, and the wing ejector inlet covers were closed. The latter choice was necessary since the wing ejector units were removed from the model and the available space was used for an internal "trombone" type of assembly employed to bridge the metric-nonmetric junction when supplying compressed air to the model.

Symbols

Longitudinal forces and moments are referred to the wind axis system, and the lateral-directional forces and moments are referred to the body axis system. All moment data are presented with respect to a center-of-gravity location on the fuselage centerline at 31.04 percent of the wing mean aerodynamic chord (at fuselage station 47.40). All dimensional data are given in U.S. Customary Units.

A_j	control-jet-exit area, ft^2
b	wing span, ft
C_A	Axial-force coefficient, Axial force/$q_\infty S$
C_D	drag coefficient, Drag/$q_\infty S$
C_L	lift coefficient, $L/q_\infty S$
C_l	rolling-moment coefficient, $l/q_\infty Sb$
C_m	pitching-moment coefficient, $m/q_\infty S\bar{c}_w$
C_N	normal-force coefficient, Normal force/$q_\infty S$
C_n	yawing-moment coefficient, $n/q_\infty Sb$
C_y	side-force coefficient, Side force/$q_\infty S$
C_p	pressure coefficient, $(p - p_\infty)/q_\infty$
c_j	wing chord at spanwise location of control jet, ft
$\bar{c}_w$	wing mean aerodynamic chord, ft
K_b	control-jet spanwise-position factor (see eq. (C6))
K_c	control-jet chordwise-position factor (see eq. (C5))
L	lift force, lb
L'	lift force due to jet thrust plus induced loading, lb, $(L)_{\text{wind on/jet on}} - (L)_{\text{wind on/jet off}}$

L_0	lift force with jet on and wind off, lb
ΔL	jet-induced lift increment, $L' - L_0$, lb
l	rolling moment, ft-lb
$l'/l_0, m'/m_0, n'/n_0$	control-jet effectiveness for rolling moment, pitching moment, and yawing moment, respectively, $\frac{(\text{Data})_{\text{wind on/jet on}} - (\text{Data})_{\text{wind on/jet off}}}{(\text{Data})_{\text{wind off/jet on}}}$
m	pitching moment, ft-lb
$\dot{m}_j$	jet mass flow rate, slugs/sec
n	yawing moment, ft-lb
p	static pressure, lb/ft^2
p_a	atmospheric pressure, lb/ft^2
p_j	jet total pressure, lb/ft^2
p_∞	free-stream static pressure, lb/ft^2
q_j	jet-exit dynamic pressure, $\frac{1}{2}\rho_j V_j^2$, lb/ft^2
q_∞	free-stream dynamic pressure, $\frac{1}{2}\rho_\infty V_\infty^2$, lb/ft^2
S	wing area, ft^2
T_j	thrust of control jet, lb
V_e	effective velocity ratio, $\sqrt{q_\infty/q_j}$
V_j	jet-exit velocity, ft/sec
V_∞	free-stream velocity, ft/sec
x_j	longitudinal distance of control jet from leading edge of local wing chord, ft
$\bar{x}_j$	longitudinal distance of control jet from center of gravity (positive ahead of C.G.), ft
x/d	distance in jet-exit diameters from jet center in free-stream direction (fig. 7)
y/d	distance in jet-exit diameters from jet center normal to both the jet and the free-stream directions (fig. 7)
y_j	spanwise distance of control jet from centerline, ft
α	angle of attack, deg
β	angle of sideslip, deg
$\delta_{e,L}$	elevon deflection on left-wing semispan, positive trailing edge down, deg
$\delta_{e,R}$	elevon deflection on right-wing semispan, positive trailing edge down, deg
ρ_j	flow density at jet exit, slugs/ft^3
ρ_∞	free-stream density, slugs/ft^3

Abbreviations:

ADEN	augmented deflector exhaust nozzle
BL	butt line
C.G.	center of gravity
ENPR	estimated nozzle pressure ratio
FS	fuselage station
NPR	nozzle pressure ratio, p_j/p_∞
STOVL	short takeoff and vertical landing
VTOL	vertical takeoff and landing

Aircraft Concept

A three-view drawing of the configuration under study is illustrated in figure 1. A description of the aircraft concept and a discussion of the intended flight modes, illustrated in figure 2, are given in appendix A. For hovering and transition flight, reaction jets are located on the wing, nose, and tail sections of the aircraft. There are five individual reaction-jet thruster units. One unit is located in the nose lower surface and is directed downward for pitch control, two downward-thrusting jets are located in the wings for combined pitch and roll control, and two sideward-thrusting jets are located on the aft fuselage for yaw control. These jets are intended to be powered by high-pressure air supplied by a compressor unit driven by a small, auxiliary gas turbine for the demonstrator aircraft and by the main engine for the operational aircraft (ref. 8) in order to achieve the flow volume and nozzle pressure ratio needed for control.

Model

The wind-tunnel model was a 15-percent-scale version of the General Dynamics E-7A STOVL fighter configuration that was previously used for free flight testing in the Langley 30- by 60-Foot Tunnel. The model was constructed of molded fiberglass,

wood, and aluminum. A list of geometric characteristics is given in table I. Model modifications yielded two distinct configurations, one for the hover and transition and the other for conventional flight. For hover and transition, the ejector inlet covers are open and the diffuser units are deployed. A photograph of the model in the hover configuration is shown in figure 3. For the tests reported herein, however, the model was reconfigured to have the diffuser units deployed and the inlet covers closed. With this arrangement, the wing ejector units were removed from the model and the space was used for an internal trombone assembly employed to bridge the metric-nonmetric junction when supplying compressed air to the model. The main engine core flow could be simulated by using a commercial ejector unit located in the main engine duct; however, for these tests this ejector unit was unpowered and the core nozzle was undeflected, thus providing an open flow-through duct.

A total of eight reaction control jets were tested as illustrated in figure 4. The control jets were supplied with compressed air that was ducted through the model using 3/8-in-diameter copper tubing. A single valve was included in each copper line as a means of controlling the mass flow rate to each control jet. During these tests, however, only the full-open valve position was used. Copper tubing from the downstream side of each valve terminated in a standard 90° elbow that was flush with the model surface and served as the reaction-jet nozzle. A static pressure tap was located in each copper line downstream of the valve for monitoring and setting test pressures. These pressures were measured using transducers mounted in the model nose.

Three alternate roll-jet locations (one at the wingtip, one at the wing trailing edge, and one on a long extension that was used for the free flight tests) were examined during this investigation. (See fig. 4.) Simple extensions, which were constructed from a length of 3/8-in-diameter copper tubing and two standard 90° elbows for each jet, were attached externally to the model surface with brackets. These extensions were mated to the baseline roll-jet exit and served to simply reposition the jet-exit location.

Tunnel and Apparatus

The tests were conducted in the Langley 12-Foot Low-Speed Tunnel. This tunnel has an octagonal test section and a conventional C-strut support system with a motorized sting assembly. The model was attached to a six-component strain gauge balance which in turn was mounted to the sting. The sting entered the model through the aft nozzle location identified in figure 2.

Compressed air was supplied to the model from pressure outlets in the tunnel floor by means of lightweight high-pressure-resistant hoses. The flexible hoses were attached to copper tubing at the rear of the sting. The copper lines external to the model were taped to the sting since the metric-nonmetric junction was internal to the model. Only two jets were tested at a given time because the trombone assembly could accommodate only two pressure lines. Internal plumbing changes permitted testing of the different control jets.

Line pressure of the compressed air supply external to the test section was displayed and monitored using several large-dial gauges. Although not included in the data recording system, readings were noted by the tunnel operator and used as reference settings. All other data including strain gauge readings and pressure transducer readings were recorded using a Hewlett-Packard 9845 computer and data acquisition system. With this system, measurements were taken at a rate of 10 samples per second for 10 sec. Average values were then computed, stored on a magnetic disc, and printed out.

Tests

All reaction control-jet configurations were tested at zero angle of attack and zero sideslip for a range of tunnel airspeeds for different pressure settings on the transducer. Each reaction jet was tested separately. Data were recorded at nominal q_∞ values of 0, 2, 3, 4, 5, and 6 lb/ft^2. Nominal pressure settings of 0, 25, 50, 75, 100, and 125 psig were employed; however, not all pressures were used for every configuration. For selected configurations, tests at several different pressure settings were also conducted over a range of angles of attack from $-2°$ to 40° and/or a range of sideslip angles from $-20°$ to 20° for a free-stream dynamic pressure q_∞ of 4 lb/ft^2. During tests of the right midwing jet, elevon effectiveness tests were also made. Chart A lists the attitude angles used for each configuration.

Prior to initiating the experimental program, several tests were made to verify the effectiveness of the trombone assembly in eliminating the tares (unwanted forces and moments) due to bridging the balance with the compressed air lines. Tests were made with the trombone assembly removed from the model, with the trombone assembly in the model but unpressurized, and with the trombone assembly in the model and pressurized at 150 psig with the valves closed. Data comparisons for the three setups showed that only insignificant differences existed, thus indicating essentially zero tare loads due to bridging the balance with the compressed air lines.

Chart A

Control moment	Jet location	Test conditions	
		α, deg	β, deg
Roll and pitch	Right midwing (baseline)	(a)	(b)
	Right-wing long extension	0	0
	Right wing at trailing edge	0	0
	Right wing at wingtip	0	0
	Left midwing (baseline)	0	0
	Left-wing long extension	0	0
Pitch up	Nose	(c)	0
Yaw left	Aft fuselage, left side	(c)	0

[a]$\alpha = -2°$, $0°$, $5°$, $10°$, $15°$, $20°$, $25°$, $30°$, $35°$, $40°$; also tested with $\delta_{e,R} = \pm 20°$.

[b]$\beta = 0°$, $\pm 5°$, $\pm 10°$, $\pm 15°$, $\pm 20°$.

[c]$\alpha = -2°$, $0°$, $5°$, $10°$, $15°$, $20°$, $25°$, $30°$, $35°$, $40°$.

Corrections

The model was tested only in the upright position in the test section, so corrections for the flow angularity were not obtained. In addition, since a majority of the tests were made at zero pitch attitude, corrections for jet-boundary effects, blockage, and support interference were not applied.

Results and Discussion

General Remarks

Because of the greater sensitivity of the balance-moment channels relative to the force channels, the moment data rather than the force data were used to compute control-jet effectiveness. The force data were examined and used as a cross-check. Thus, pitching-moment data were used for the nose-jet analysis and yawing-moment data were used for the yaw-jet analysis. Since the other jet configurations involved both pitch and roll control, only the rolling-moment data were employed to take advantage of the sensitivity of the roll balance channel.

Control-jet effectiveness as used herein is defined as a ratio of the moment produced by operating the control jet under transition conditions (wind on) to the moment produced by the jet during hover (wind off). Wind-on data runs were made varying either tunnel airspeed or model attitude angle usually while holding constant the pressure to the control jet as measured by the transducer. In place of a pressure setting as the data identification on the figures, a value of estimated nozzle pressure ratio (ENPR) was employed that was calculated for the wind-off condition as described in appendix B.

Baseline Roll Jets

Force and moment data for $\alpha = 0°$ and $\beta = 0°$ were obtained through the q_∞ range for the baseline roll jets operating at different pressure settings. Measurements were made for both the right-wing jet and the left-wing jet operating individually. Figure 5 shows representative plots of the aerodynamic coefficients versus free-steam dynamic pressure with ENPR as a parameter. During the tests, two independent data sets were obtained for an ENPR value of 1.0. Both sets are included to indicate the repeatability of the data.

Using the measured rolling-moment values for wind-on and wind-off conditions, values of the effectiveness of the control jets as a function of the effective velocity ratio V_e were obtained and these results are given in figure 6. Values of the estimated velocity ratio V_e used in figure 6 were obtained by the method indicated in appendix B.

An examination of the data in figure 6 indicates that during transition flight a substantial reduction occurs in the effectiveness of the control jets with increasing V_e. (Increasing V_e corresponds to an increase in forward speed for a given supply pressure to the control jets.) This result is in agreement with previous studies and shows the influence of the suck-down pressure field aft of the control-jet efflux. (For reader convenience, a sketch of the pressure field about a jet exhausting at 90° to a crossflow is given in figure 7 to illustrate the large surface area to the side and to the rear of the jet influenced by negative pressures that reduce control-jet effectiveness. The sketch was made from data figures presented in refs. 2, 9, and 10.) Also shown in figure 6 are two calculated curves obtained using the method presented in reference 1 and briefly summarized in appendix C. As can be seen, the calculated results in figure 6 are in fairly good agreement with the experimental data when considering the scatter shown. It should be noted that the rolling-moment ratio l'/l_0 used in figure 6 can also be used as an approximation to the lift ratio L'/L_0.

Longitudinal aerodynamic characteristics of the model through the angle-of-attack range with the baseline right-wing control jet operating are presented in figure 8. Both wind axis data and body axis data are provided for convenience. In addition, the corresponding rolling-moment data with the control jet operating are presented in figure 9. An examination of the latter data indicated that varying the angle of attack had little effect on the control-jet effectiveness for the baseline jet location.

The effect of sideslip angle β on the model rolling-moment coefficient with the right-wing control jet operating at several pressures is presented in figure 10. Results are presented through the sideslip range from $-20°$ to $20°$ at three different angles of attack and two tunnel dynamic pressure settings. A change in control-jet effectiveness with sideslip was anticipated because of the rotation of the model surface relative to the pressure field. This anticipated effect on C_l is not apparent in the data. Large effects of sideslip that involve sideslip angles of $-30°$ to $30°$ and jet pressure ratios up to 6.0 have been noted in other studies such as reference 7.

Rolling-moment-coefficient data are presented in figure 11 for several elevon deflections with the control jet operating. Only the right elevon and right-wing baseline jet were employed for these tests. An examination of the data shows that a loss in elevon roll-control power occurs for angles of attack above $25°$. Also, the data indicate that no aerodynamic interference or coupling exists between the two controls. Some previous studies on other configurations have shown similar results (ref. 7).

Wing-Trailing-Edge Roll Jet

Force and moment data were obtained through the q_∞ range at $\alpha = 0°$ and $\beta = 0°$ for the model with the right-wing control jet located at the wing trailing edge and operating at various pressure settings. A simple extension mounted external to the wing lower surface was employed to reposition the jet exit from the baseline location. This extension was mounted in a chordwise direction and was attached to the wing such that the plane of the jet exit was tangent to the wing upper surface. For this test the jet efflux was discharged upward above the wing and normal to the wing chord plane. (See fig. 4(b).) From using the rolling-moment data, control-jet-effectiveness results were obtained and are presented in figure 12. Also shown are calculated curves using the equations in appendix C.

The calculated curve of figure 12 predicts an increase in control-jet effectiveness as V_e increases. Because of the jet location, the suck-down pressure field aft of the jet efflux has been moved off the wing surface, thereby leaving only the positive pressure field forward of the jet to augment the jet thrust and hence increase the jet effectiveness. The comparison of measured and calculated results shown in figure 12 is not good. The measured data show considerable scatter and an effectiveness value less than 1.0 for some V_e values. Note that the calculated curve applies for conditions when the center of the jet is at the wing trailing edge. However, the measured data were obtained with the jet center slightly aft of the trailing edge with the circular jet exit tangent to the trailing edge. Some of the difference between calculated and measured results could be due to the difference in jet locations.

Wingtip Roll Jet

Tests through the q_∞ range with the model at $\alpha = 0°$ and $\beta = 0°$ were made with the control jet located at the right wingtip and operated at several pressure settings. An extension mounted to the wing lower surface was used to reposition the jet exit from the baseline location. The extension was mounted in a spanwise direction with the plane of the jet exit tangent to the wing upper surface. The jet efflux was discharged upward above the wing and normal to the wing chord plane. (See fig. 4(b).) As in the previous cases, only the rolling-moment data were used to obtain values for control-jet effectiveness. These results are given in figure 13 along with calculated curves using the equations in appendix C.

A much smaller loss in control-jet effectiveness predicted by the empirical equations in appendix C is noticeable in figure 13 when compared with that for the baseline jet location given in figure 6. This difference is due to the influence of the jet spanwise position factor K_b. The comparison of measured and calculated results shown in figure 13 is not very good with scatter evident in the measured data. Similar to the case with the jet at the wing trailing edge, the circular exit of the wingtip jet was positioned tangent to the wingtip although the calculations were made for the center of the jet located at the tip. The physical arrangement tested could affect the measured values and thus influence the comparison.

Additional tests were made at $\alpha = 0°$ and $q_\infty = 4$ lb/ft^2 through the sideslip range from $-20°$ to $20°$ for several jet pressure settings. These tests were made to examine the effect, if any, on control-jet effectiveness due to shifting the induced pressure field on the wing with sideslip angle as was done for the baseline control-jet location. These tests indicated no effect of sideslip angle for the β range tested.

Roll Jets on Long Extensions

Data were obtained through the q_∞ range at $\alpha = 0°$ and $\beta = 0°$ for the model with the control jets located some distance beyond the wingtips and operated at several pressure settings. Long extensions were mounted in a spanwise direction external to the wing lower surface to reposition the jet exit from the baseline location. For these tests the jet efflux was directed downward similar to the baseline case. (See fig. 4(b).) Tests were made with the extension mounted on the right wing and then on the left wing. The particular extensions used were those

previously employed during the model free flight tests in the Langley 30- by 60-Foot Tunnel as an easy way of increasing the model roll-control power for the same pressure settings. Using only the rolling-moment data from these tests, values of control-jet effectiveness were obtained and the results are presented in figure 14. An examination of the data in figure 14 indicates no change in control-jet effectiveness with increasing V_e from that at the hover conditions ($V_e = 0$). Although no calculated curve is provided, a value of l'/l_0 of 1.0 should apply over the range since no wing surface exists in the immediate vicinity of the jet.

Nose Jet

Tests were made through the q_∞ range for the model at $\alpha = 0°$ and $\beta = 0°$ with various pressure settings on the nose jet. Using the pitching-moment data from these tests, values of control-jet effectiveness as a function of V_e were obtained and the results are given in figure 15. The data indicated that a loss in control-jet effectiveness with increasing V_e from the hover condition was undoubtedly due to the suck-down pressure field acting on the fuselage aft of the jet exit. The loss shown in figure 15, however, is not as large as that obtained for the baseline roll jet for comparable values of V_e. The result is probably due to the smaller surface area in the vicinity of the jet and, to a lesser extent, to the local surface curvature of the model. A calculated curve is not shown in figure 15 since, at present, the empirical method of reference 1 (summarized in appendix C) has not been extended to jet-fuselage combinations.

Yaw Jets

Data were obtained through the q_∞ range for the model at $\alpha = 0°$ and $\beta = 0°$ with various pressure settings on the left yaw jet. Using the yawing-moment data, values of control-jet effectiveness were obtained and are presented in figure 16 as a function of V_e. The data indicate a slight loss in effectiveness for all pressure settings except for the lowest value tested. Note that a large amount of scatter was obtained for this particular pressure setting. As in the case of the nose jet, empirical values for comparison could not be calculated since methods for jet-fuselage arrangements are not available.

Since the yaw jets were located only a short distance behind the wing trailing edge, tests through the angle-of-attack range were made at several pressure settings to examine possible changes in jet interference effects with angle of attack. Figure 17 presents the lateral coefficients C_y, C_n, and C_l obtained from these tests. Of particular interest are the data indicating the presence of a rolling moment above $\alpha = 15°$ that does not seem associated with the C_y and C_n results. Accordingly, the normal-force increments ΔC_N were obtained from data for the two pressure settings, and these increments are presented in figure 18. The results indicate that changes in loading on the left-wing semispan due to the presence of the discharging yaw jet contribute to the rolling moments that were measured.

Conclusions

A brief wind-tunnel investigation was conducted in the Langley 12-Foot Low-Speed Tunnel to determine reaction control-jet effectiveness and some aerodynamic characteristics applicable to transition flight on a 15-percent-scale model of a STOVL single-engine fighter concept developed by General Dynamics and designated as configuration E-7A. In addition to the baseline geometry, several alternate roll-jet locations were tested. The various control jets were powered by compressed air, and each jet was tested individually. A total of eight different jet locations were examined. Where possible, the measured data were compared with values calculated using an available empirical method. Results of the study are summarized as follows:

1. Roll-control jets at the design location on the wing semispan (baseline case) showed a significant loss in control-jet effectiveness as effective velocity ratio V_e increased. (Increasing V_e corresponds to an increase in speed during transition flight.) The loss in effectiveness was caused by the presence of a suck-down induced pressure field acting on the wing surface aft of the jet exit. A comparison of the experimental data with calculated values showed fairly good agreement for this jet location.

2. For the ranges tested, changes in sideslip angle, angle of attack, and elevon deflection have little effect on the roll-control jet data for the design roll-jet location.

3. Control-jet-effectiveness values determined from tests with the roll-control jet located either at the wing trailing edge or at the wingtip involved smaller losses than those obtained with the baseline jet location; however, sufficient scatter existed so that the data were not conclusive in supporting the empirical calculations.

4. Control-jet effectiveness for transition flight was found to be invariant from that at the hover condition when the roll-control jet was positioned spanwise some distance outboard of the wingtip.

5. Control-jet effectiveness of the nose jet decreased as effective velocity ratio V_e increased; however, the loss in effectiveness was less than that for the baseline roll jet, undoubtedly because of the

smaller surface area influenced by the jet-induced pressure field.

6. Control-jet effectiveness of the yaw jet showed, in general, a slight loss for the transition flight regime from that at the hover condition. In addition, because the yaw jets were located only a short distance aft of the wing trailing edge, undesirable rolling moments due to loading changes on the wing occurred at angles of attack above 15°.

NASA Langley Research Center
Hampton, VA 23665-5225
September 27, 1989

Appendix A

Aircraft Description and Operational Modes

A three-view drawing of the E-7A configuration is presented in figure 1. The design employs an ejector-augmentor system driven by engine bypass air that is located in the wing root section near the apex of a large 60° clipped-delta wing. A two-dimensional ADEN-type core nozzle is located rearward on the undersurface of the aircraft for vectoring the hot main-engine exhaust. The long diffuser units of the wing ejector-augmentor system shown in the front view are employed to improve the efficiency of the design. As illustrated, the aircraft would operate in the hover and transition flight modes. For high-speed flight, the aircraft is reconfigured. The diffuser units are collapsed and stowed, and the ejector inlet covers are closed. For hover, attitude control is provided by reaction control jets located in the nose, wing, and tail sections of the aircraft. For conventional flight, control is provided by elevons and a rudder. During transition, both systems are used.

Figure 2 illustrates the proposed method of achieving STOVL capability. For hovering flight, all engine bypass air is ducted forward to the wing ejectors. The ejector-augmentor combination induces a large secondary mass flow that increases the thrust output of the system. The core nozzle is deflected to turn the core flow 90° downward. During transition, the core nozzle angle is varied and the engine bypass air is modulated between the wing ejector system and the aft nozzle. For conventional flight, all engine bypass air is directed rearward through the aft nozzle.

Appendix B

Equations Used In Data Reduction

Because of the geometry used for the control jets in the model, the flow exiting the nozzles was very distorted. For this reason the following simplified mathematical expressions, which assume incompressible flow, were employed.

Determining Values of V_e

To determine the values of effective velocity ratio V_e, the wind-off values of the measured moment (rolling moment l used for illustration) and the geometric moment arm may be used to compute the jet thrust by

$$T_j = l/y_j \tag{B1}$$

where it is recalled that

$$\left.\begin{aligned} T_j &= \dot{m}_j V_j \\ &= \rho_j A_j V_j V_j \\ &= 2A_j q_j \end{aligned}\right\} \tag{B2}$$

Therefore,

$$q_j = T_j/2A_j \tag{B3}$$

Finally,

$$\left.\begin{aligned} V_e &= \sqrt{\frac{q_\infty}{q_j}} \\ &= \sqrt{\frac{\rho_\infty}{\rho_j}}\frac{V_\infty}{V_j} \end{aligned}\right\} \tag{B4}$$

where q_∞ is measured and q_j is calculated from equation (B3).

Computing ENPR

To compute the estimated nozzle pressure ratio ENPR, let

$$\text{ENPR} = \frac{p_a + q_j}{p_a} \tag{B5}$$

where q_j is calculated from equation (B3).

Appendix C

Estimation of Control-Jet Effectiveness

Empirical equations predicting the induced lift loss of a reaction control jet exhausting into a cross-flow are presented in reference 1. These equations are presented here for convenience since they were used in the comparisons presented herein.

The empirical method assumes that the lift loss due to jet-induced effects consists of two terms which are designated by the subscripts o and p. Thus,

$$\frac{\Delta L}{T_j} = \left(\frac{\Delta L}{T_j}\right)_o + \left(\frac{\Delta L}{T_j}\right)_p \tag{C1}$$

where

$$\left(\frac{\Delta L}{T_j}\right)_o = (3V_e^3 - 2.4V_e^2)\left(\frac{S}{A_j}\right)^{0.5} + 0.41V_e^{2.2}\left(\frac{S}{A_j}\right)^{0.688} \tag{C2}$$

If

$$\frac{p_j}{p_\infty} \leq 1.893$$

then

$$\left(\frac{\Delta L}{T_j}\right)_p = 0$$

and if

$$\frac{p_j}{p_\infty} > 1.893$$

then

$$\left(\frac{\Delta L}{T_j}\right)_p = -0.17V_e\left(\frac{S}{A_j}\right)^{0.42}\left(\frac{p_j}{p_\infty} - 1.893\right)^{0.75} \tag{C3}$$

The increment in roll-control moment can be written as

$$\Delta l = T_j y_j \frac{\Delta L}{T_j} \tag{C4}$$

The above equations, as indicated in reference 1, apply to values of velocity ratio V_e up to 0.1, to values of S/A_j up to about 7000, and to jet pressure ratios p_j/p_∞ up to about 45.

To adjust the above method for control-jet locations near the wingtip and near the wing trailing edge, the factors K_c and K_b were proposed in reference 1 as follows:

$$K_c = 1 - 1.23\left(\frac{x_j}{c_j}\right)^4 \tag{C5}$$

$$K_b = 1 - 0.8\left(\frac{y_j}{b/2}\right)^{13} \tag{C6}$$

The total expression for the estimated increment in rolling moment is then given by

$$\Delta l = T_j y_j \left[\left(\frac{\Delta L}{T_j}\right)_o + \left(\frac{\Delta L}{T_j}\right)_p\right] K_c K_b \tag{C7}$$

References

1. Kuhn, Richard E.: A Method for Estimating Jet Reaction Control Effectiveness. *A Collection of Technical Papers—AIAA 4th Applied Aerodynamics Conference,* June 1986, pp. 237–242. (Available as AIAA-86-1805.)
2. Fearn, Richard L.; and Weston, Robert P.: *Induced Velocity Field of a Jet in a Crossflow.* NASA TP-1087, 1978.
3. Aoyagi, Kiyoshi; and Snyder, Philip K.: Experimental Investigation of a Jet Inclined to a Subsonic Crossflow. AIAA-81-2610, Dec. 1981.
4. Kotansky, Donald R.: Jet Flowfields. *Special Course on V/STOL Aerodynamics,* AGARD-R-710, Apr. 1984, pp. 7-1–7-48.
5. Wood, M. N.: Jet V/STOL Aircraft Aerodynamics. *Ann. N.Y. Acad. Sci.,* vol. 154, article 2, Nov. 22, 1968, pp. 893–920.
6. Maskew, B.; Strash, D.; Nathman, J.; and Dvorak, F. A.: *Investigation To Advance Prediction Techniques of the Low-Speed Aerodynamics of V/STOL Aircraft.* NASA CR-166479, 1983.
7. Spreemann, Kenneth P.: *Free-Stream Interference Effects on Effectiveness of Control Jets Near the Wing Tip of a VTOL Aircraft Model.* NASA TN D-4084, 1967.
8. Foley, W. H.; Sheridan, A. E.; and Smith, C. W.: *Study of Aerodynamic Technology for Single-Cruise-Engine V/STOL Fighter/Attack Aircraft.* NASA CR-166268, 1982.
9. Fearn, Richard; and Weston, Robert P.: Vorticity Associated With a Jet in a Cross Flow. *AIAA J.,* vol. 12, no. 12, Dec. 1974, pp. 1666–1671.
10. Vogler, Raymond D.: *Surface Pressure Distributions Induced on a Flat Plate by a Cold Air Jet Issuing Perpendicularly From the Plate and Normal to a Low-Speed Free-Stream Flow.* NASA TN D-1629, 1963.

Table I. Model Geometric Characteristics

Wing:	
Area, ft^2	14.1885
Aspect ratio	1.665
Taper ratio	0.115
Span, in.	58.320
Root chord, in.	62.860
Tip chord, in.	7.212
Mean aerodynamic chord (MAC), in.	42.402
Leading-edge station of MAC, in.	FS 34.239
Span station of MAC, in.	BL 10.720
Leading-edge sweep, deg	60
Trailing-edge sweep, deg	−10
Airfoil	NACA 64A004
Incidence, deg	0
Dihedral, deg	0
Twist, deg	0
Elevon area, ft^2	1.7026
Vertical tail:	
Area, ft^2	1.2319
Aspect ratio	1.294
Taper ratio	0.437
Height, in.	15.150
Root chord, in.	16.293
Tip chord, in.	7.125
Leading-edge sweep, deg	47.5
Airfoil:	
Root	5.3-percent-thick biconvex
Tip	3.0-percent-thick biconvex
Rudder area, ft^2	0.2621
Fuselage:	
Length (nose boom removed), in.	84.5415

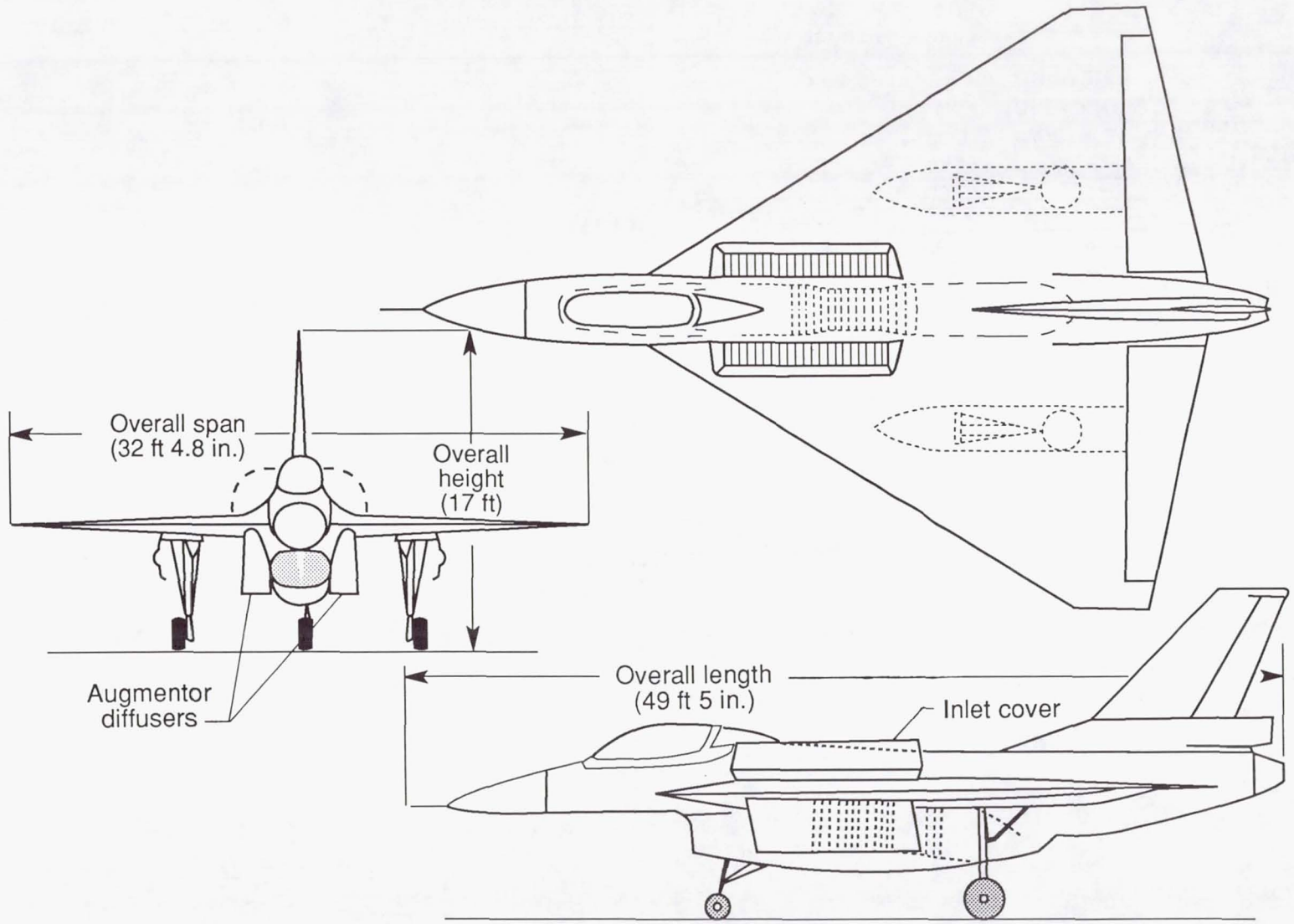

Figure 1. The General Dynamics E-7A configuration.

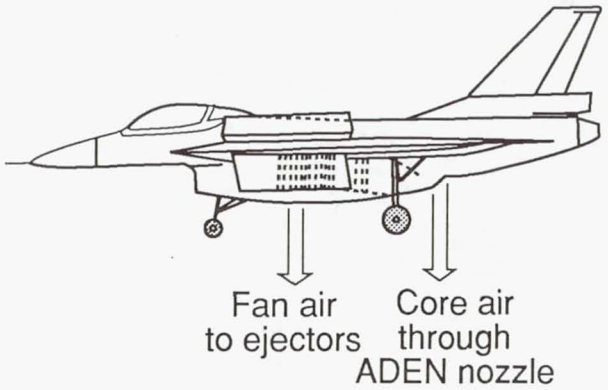

(a) Hovering flight.

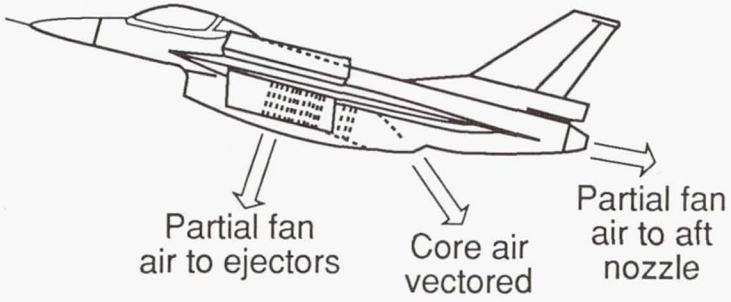

(b) Short-takeoff-and-transition flight.

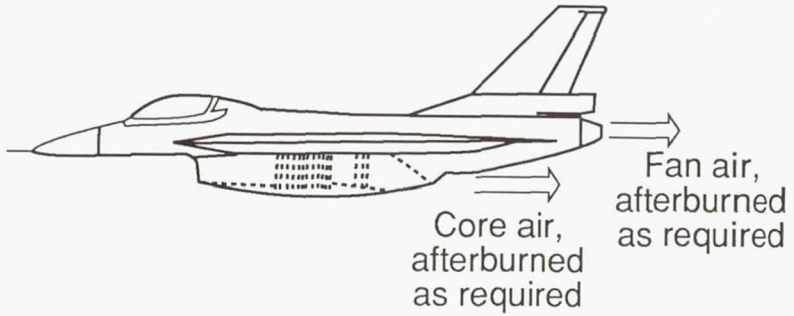

(c) Conventional flight.

Figure 2. Modes of operation of the E-7A.

L-85-5629

Figure 3. Photograph of 15-percent-scale E-7A model.

Jet Locations		
Control jet	$\bar{x}_j$, in.	y_j, in.
Baseline jets	-20.240	±16.160
Trailing-edge jet	-28.115	+16.160
Wingtip jet	-20.240	+29.348
Jets on long extension	-20.240	±35.535
Nose jet	+35.900	0
Yaw jet	[a]-32.350	(b)

[a] Jet exit 1.50 in. aft of wing trailing edge.
[b] Exit at fuselage surface with jet directed through centerline parallel to lateral direction.

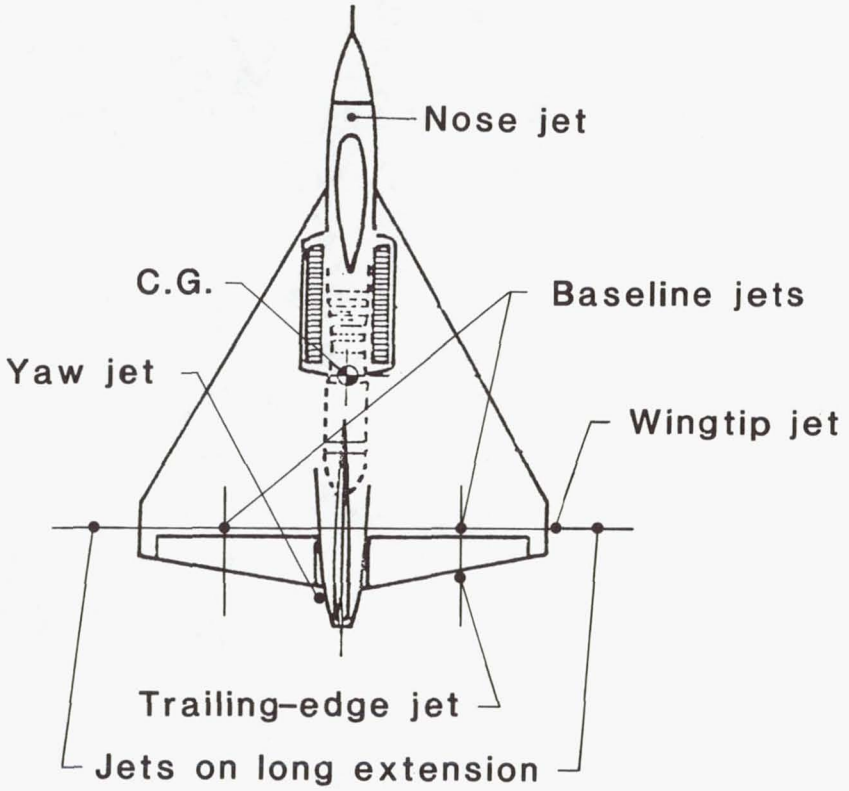

(a) Planview of control-jet locations.

Figure 4. Control-jet locations tested. Dimensions are given in inches.

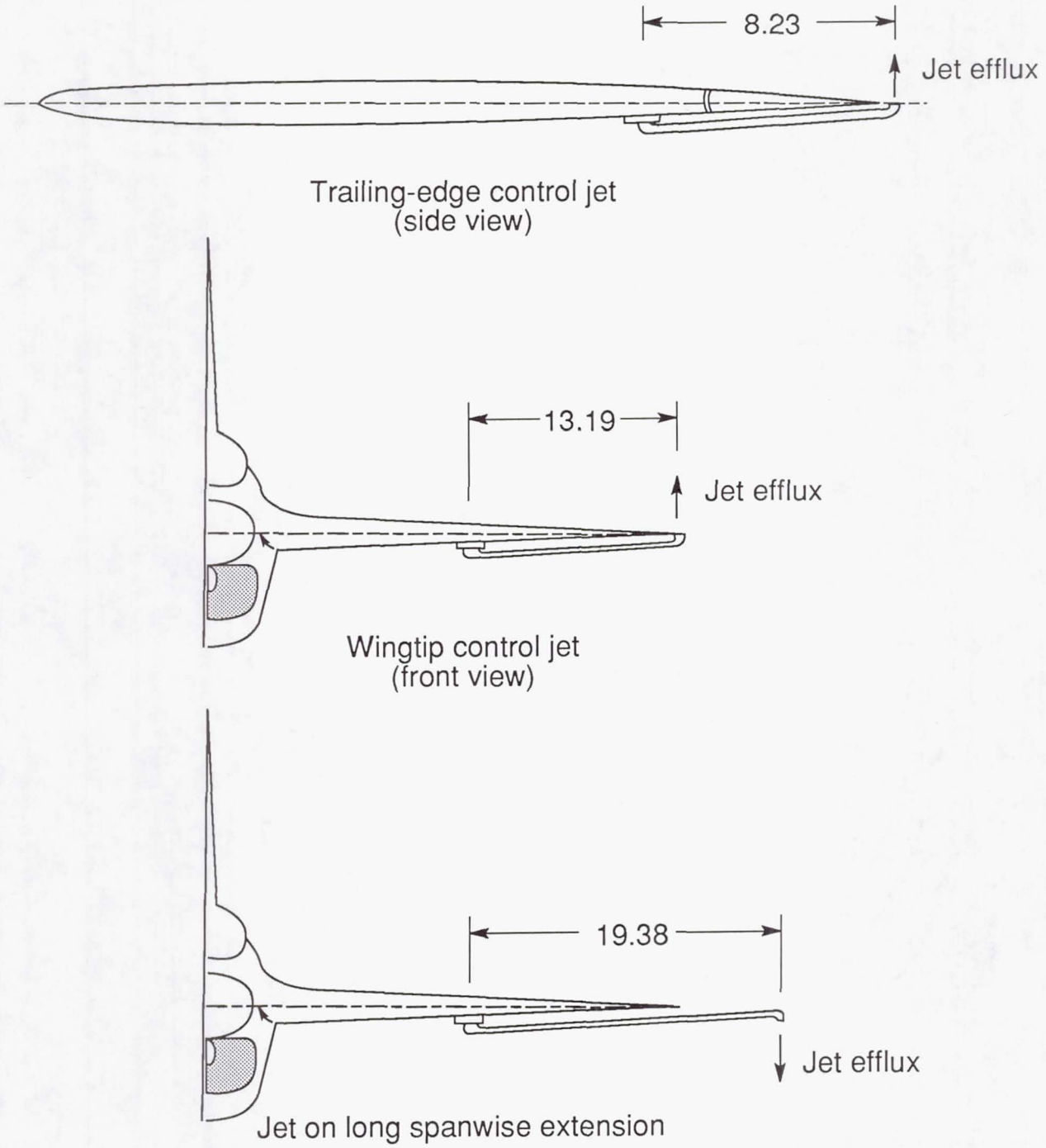

(b) Sketches of alternate jet locations.

Figure 4. Concluded.

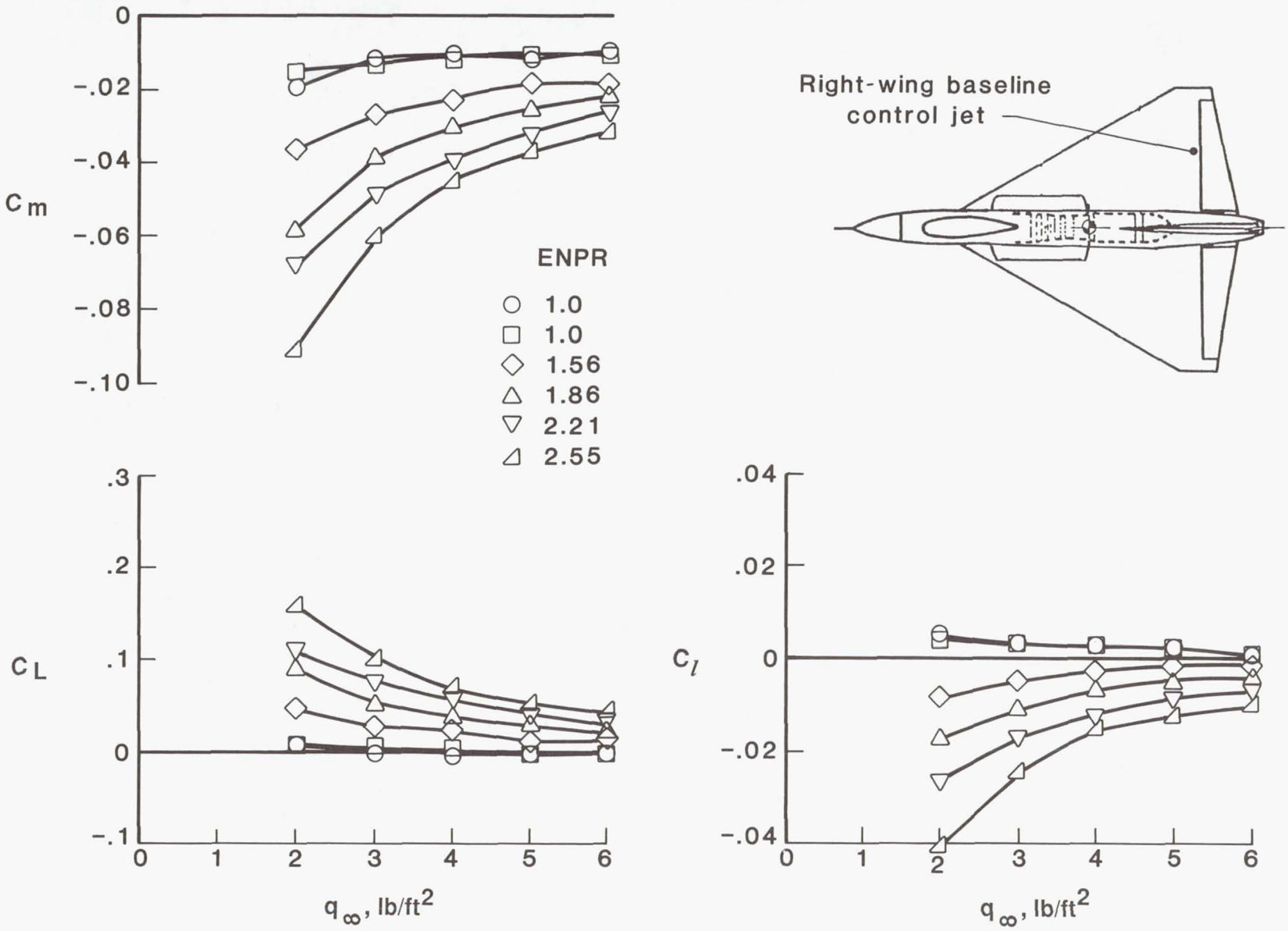

Figure 5. Effect of free-stream dynamic pressure on model with design right-wing control jet operating at several pressure settings. $\alpha = 0°$; $\beta = 0°$; $\delta_{e,L} = \delta_{e,R} = 0°$.

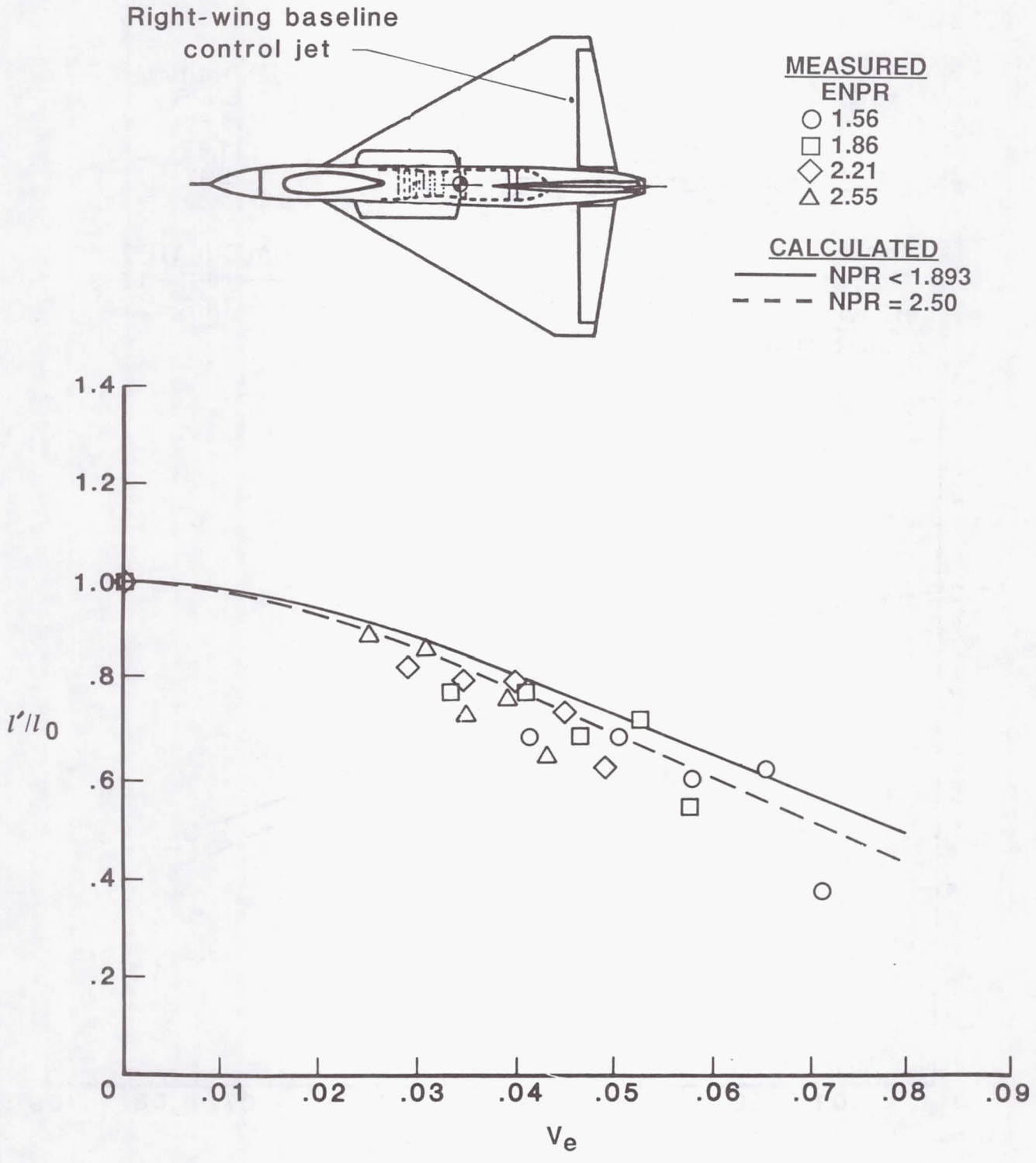

(a) Right-wing roll jet.

Figure 6. Effectiveness of baseline roll jets for transition conditions. $\alpha = 0°$; $\beta = 0°$; $\delta_{e,L} = \delta_{e,R} = 0°$.

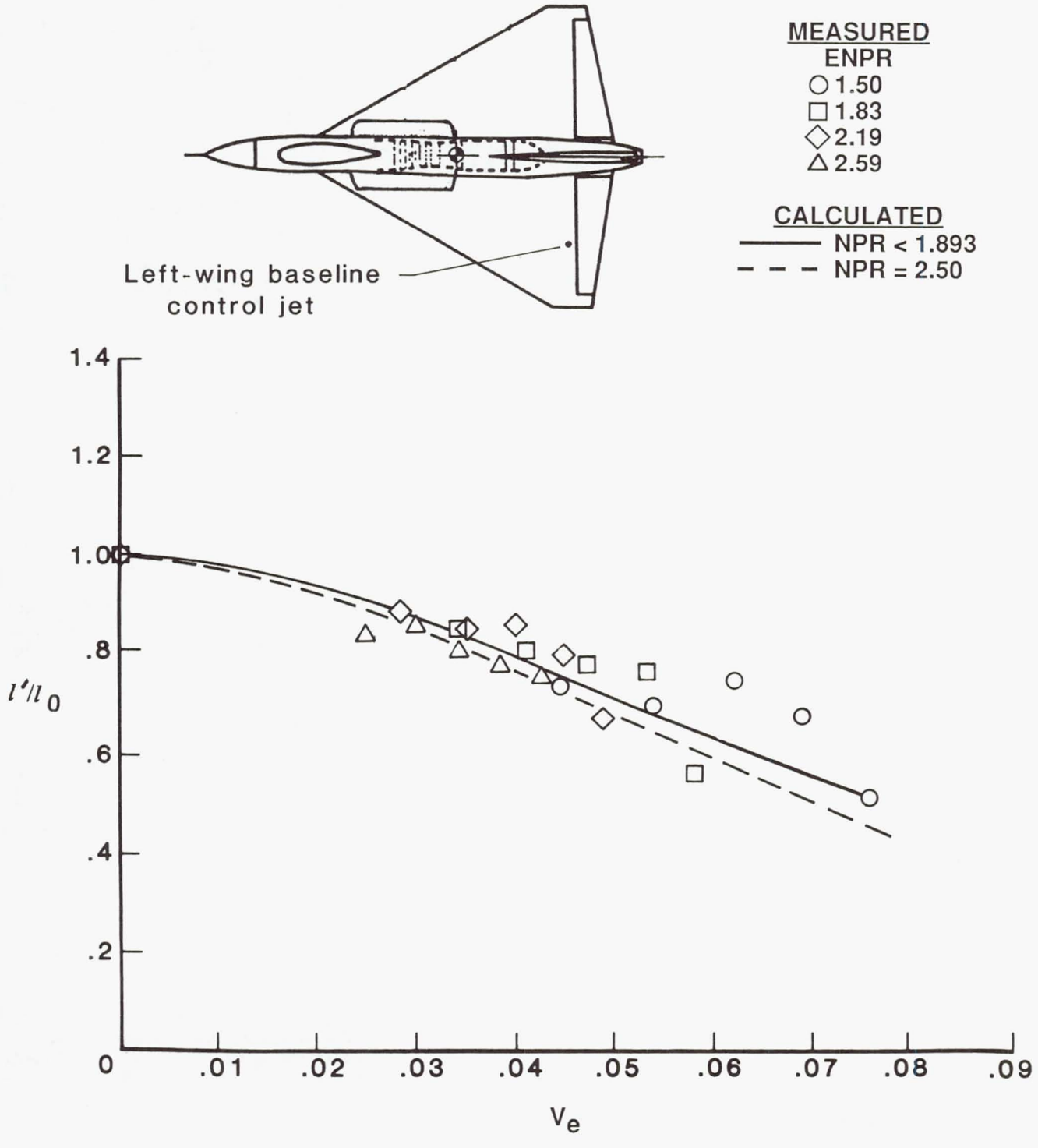

(b) Left-wing roll jet.

Figure 6. Continued.

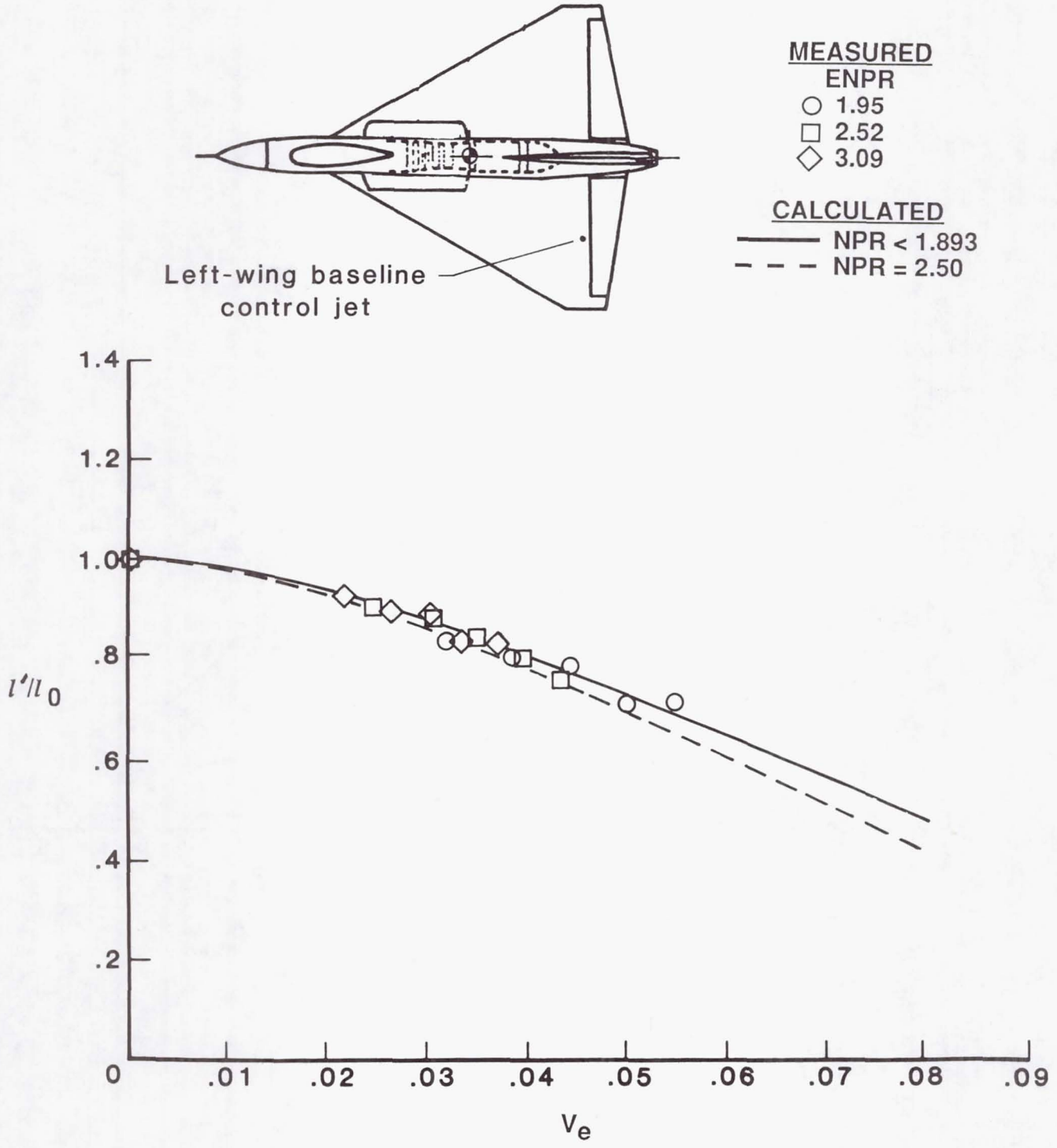

(c) Left-wing roll jet.

Figure 6. Concluded.

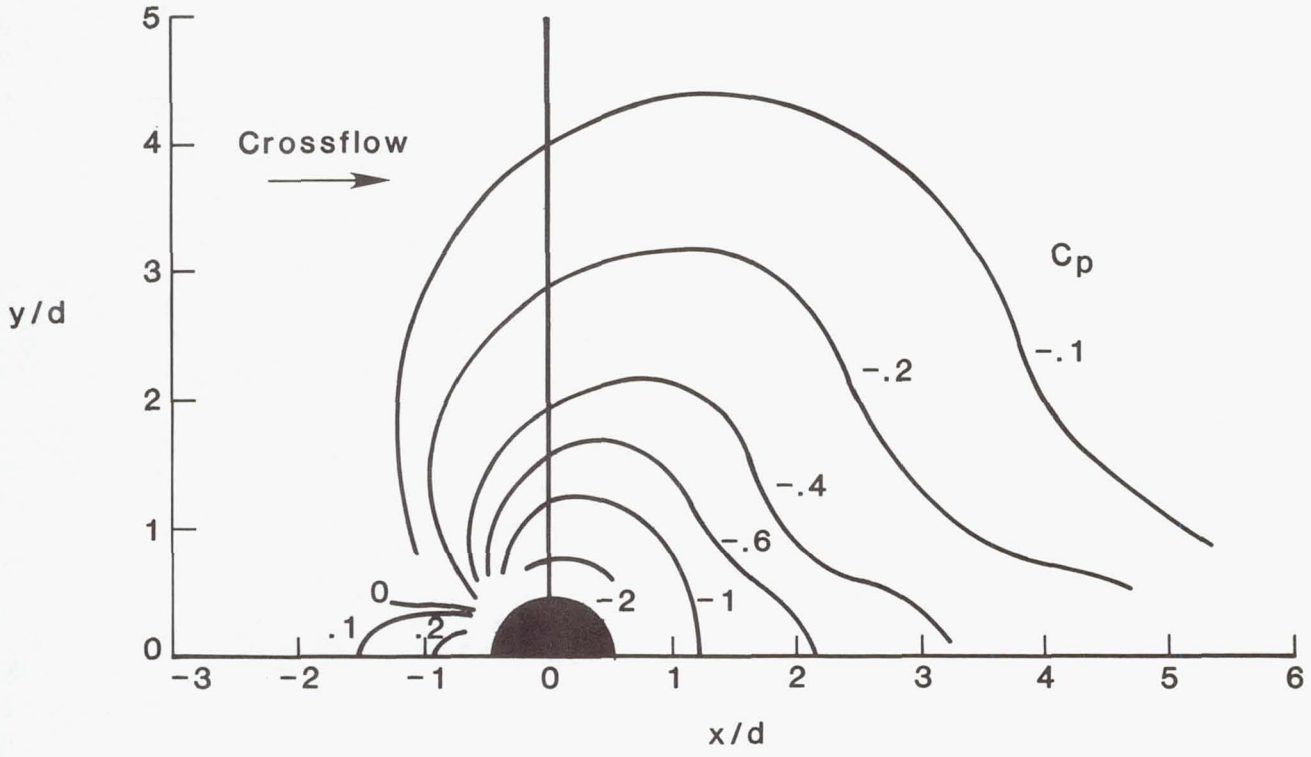

Figure 7. Planview sketch of constant pressure contours on flat plate at zero angle of attack with circular jet exiting at 90° to free stream. (See refs. 2, 9, and 10.)

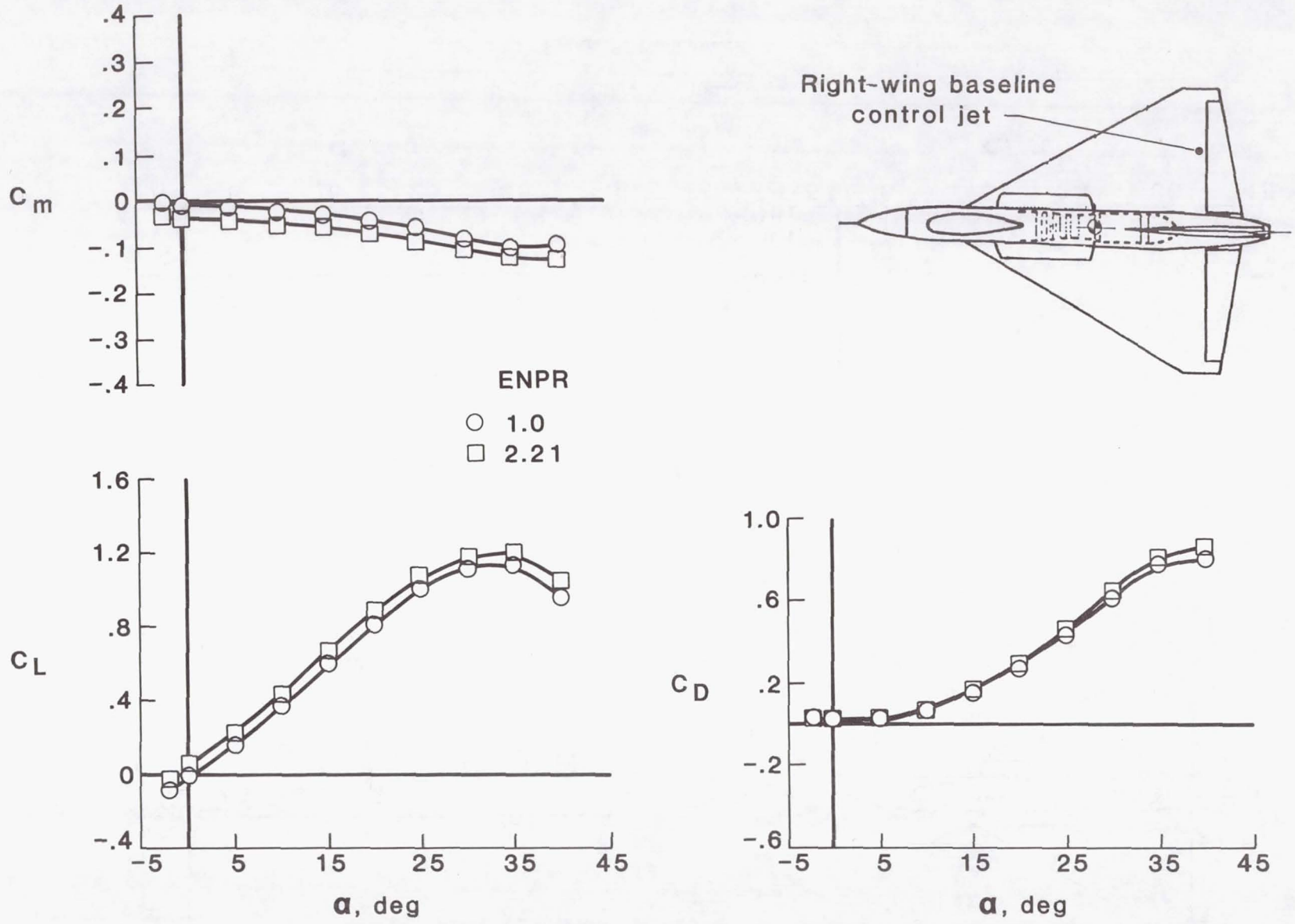

(a) Wind axis data.

Figure 8. Effect of angle of attack on longitudinal aerodynamic characteristics with and without the right-wing baseline roll jet operating. $\alpha = 0°$; $\beta = 0°$; $\delta_{e,L} = \delta_{e,R} = 0°$; and $q_\infty = 4$ lb/ft^2.

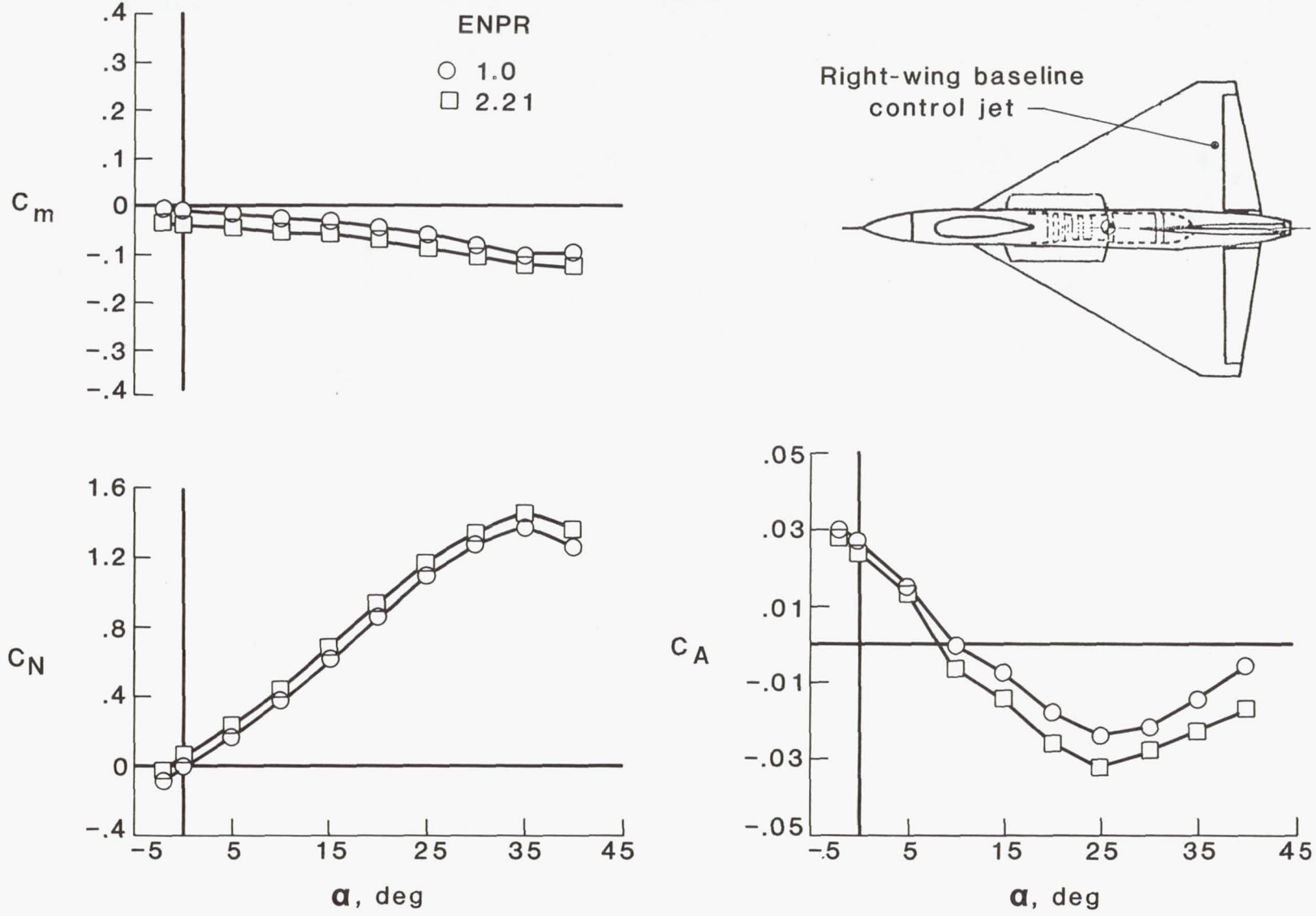

(b) Body axis data.

Figure 8. Concluded.

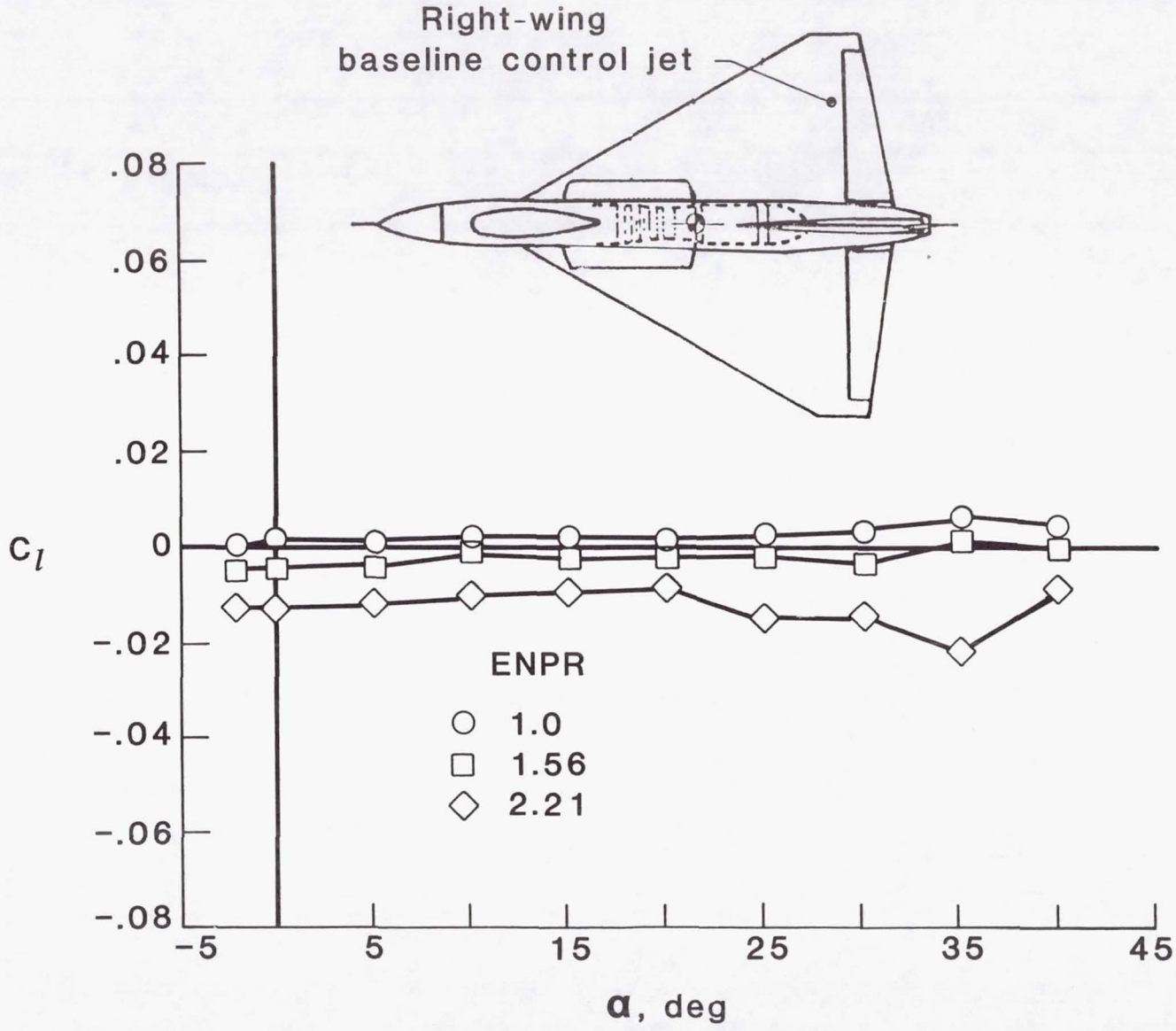

Figure 9. Variation of model rolling-moment coefficient with right-wing baseline control jet operating at several pressure settings with $q_\infty = 4$ lb/ft^2.

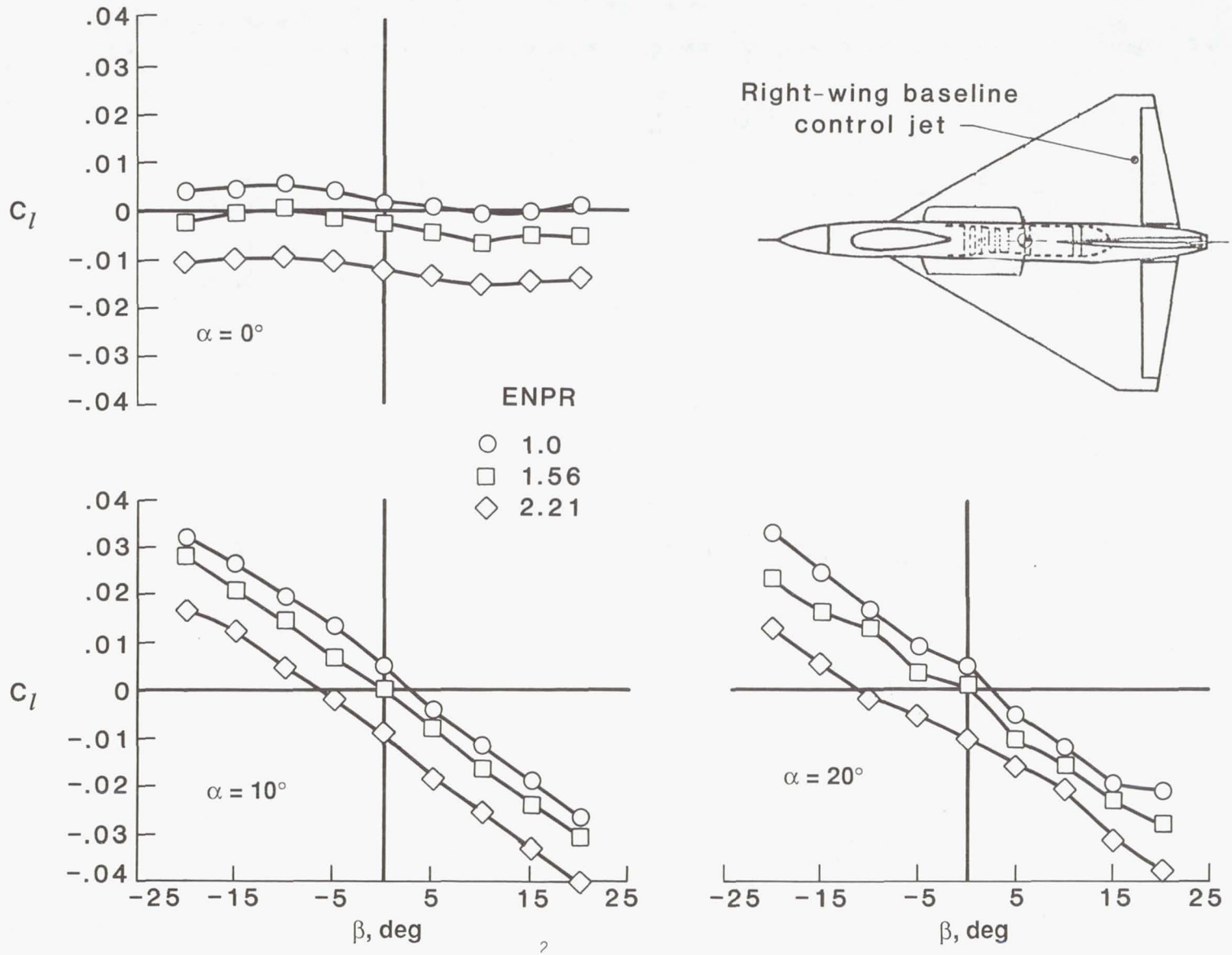

(a) $q_\infty = 4$ lb/ft^2.

Figure 10. Effect of sideslip angle on model rolling-moment coefficient with right-wing baseline control jet operating at several pressure settings.

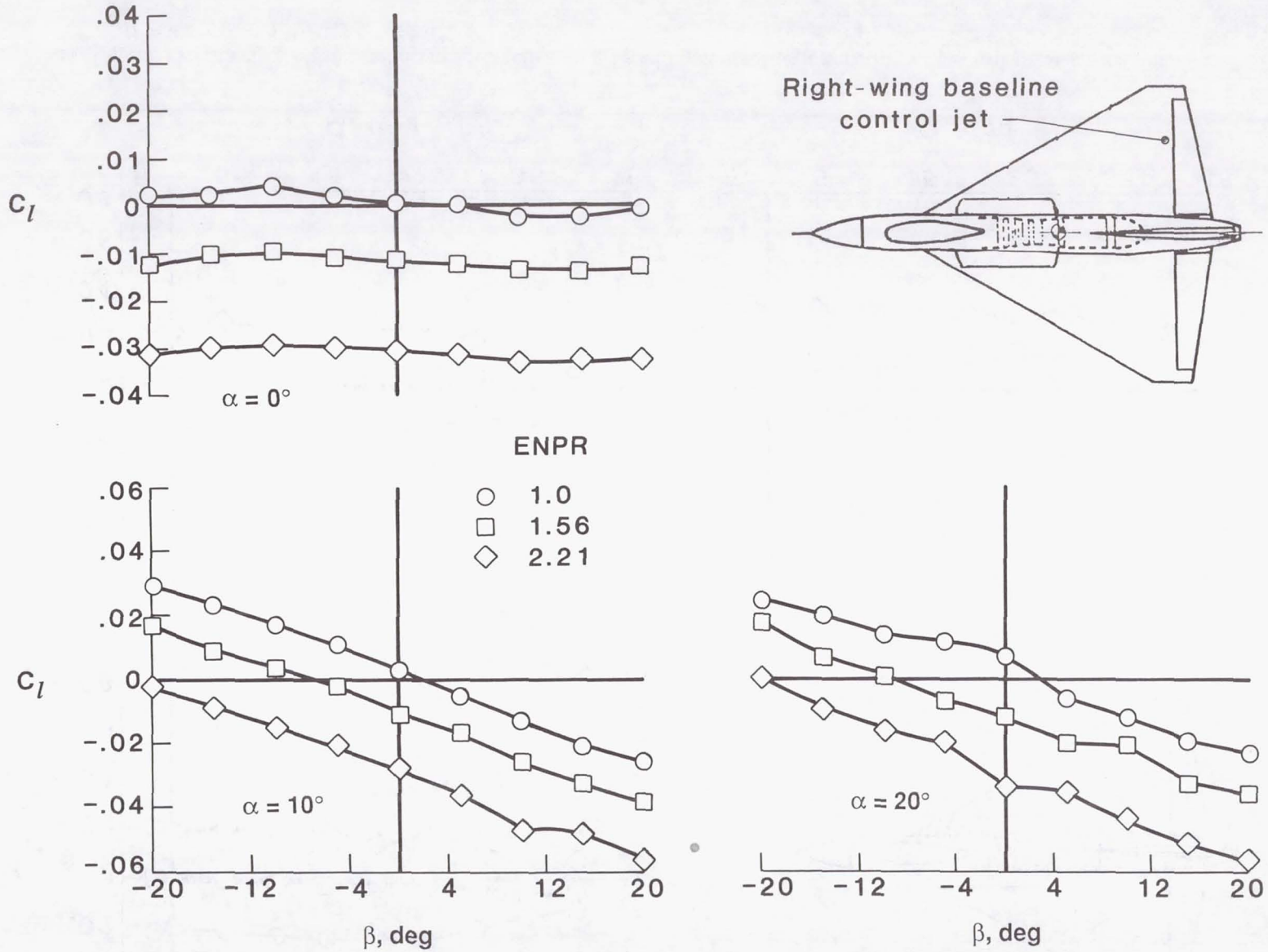

(b) $q_\infty = 2$ lb/ft^2.

Figure 10. Concluded.

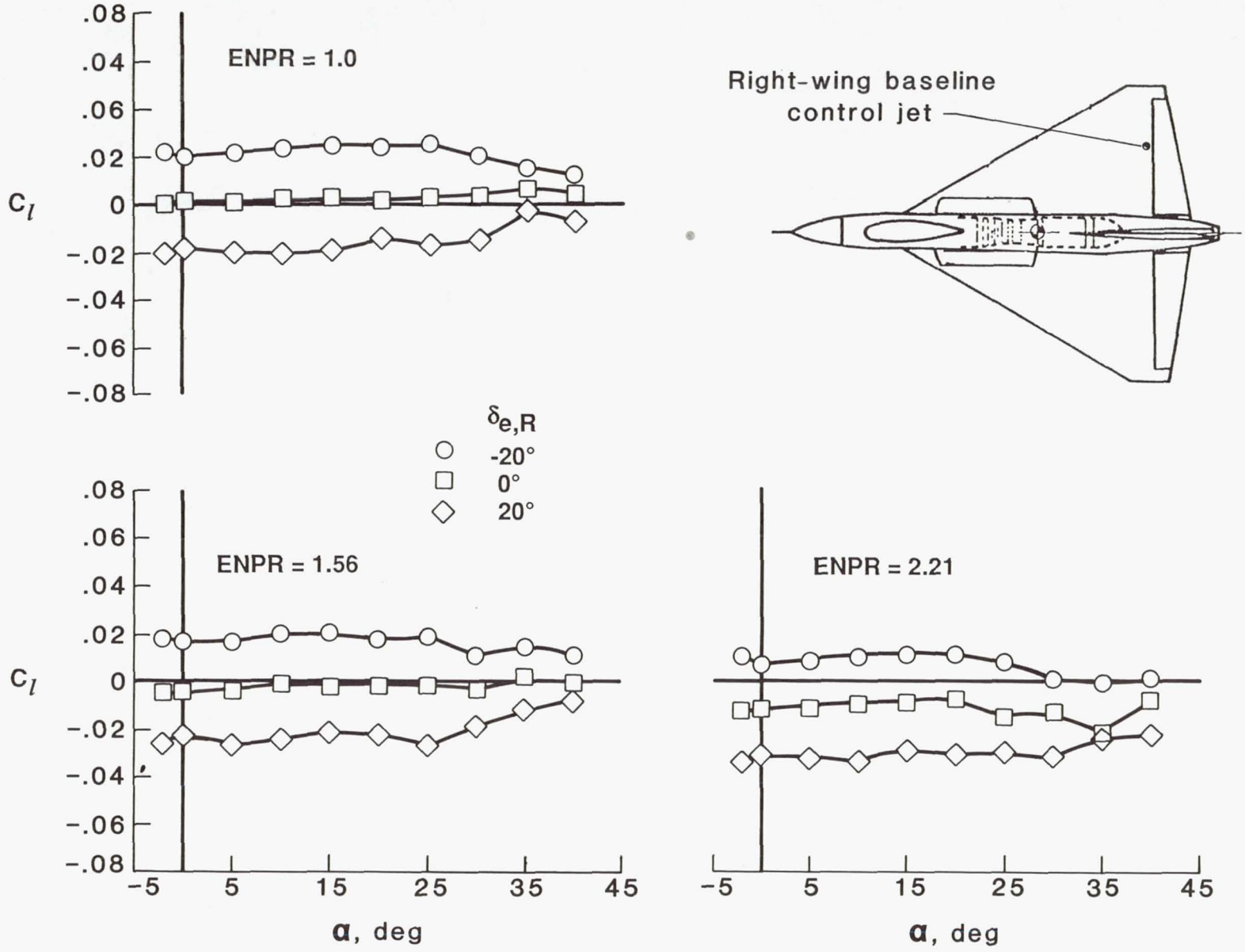

Figure 11. Effect of elevon deflection for right-wing baseline control jet operating at several pressure settings. $\beta = 0°$; $q_\infty = 4$ lb/ft^2; $\delta_{e,L} = 0°$.

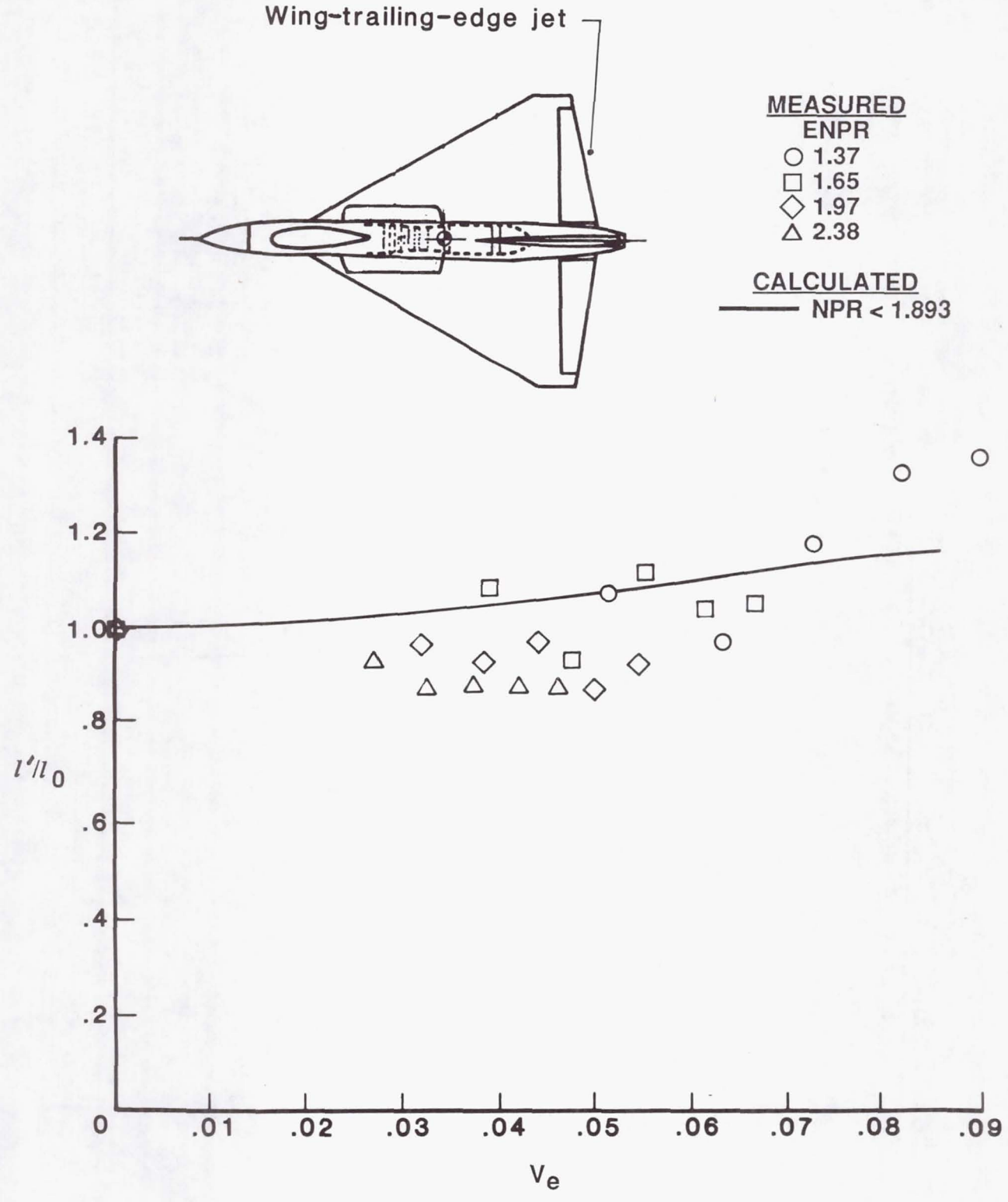

Figure 12. Effectiveness of trailing-edge roll jet for transition conditions. $\alpha = 0°$; $\beta = 0°$; $\delta_{e,L} = \delta_{e,R} = 0°$.

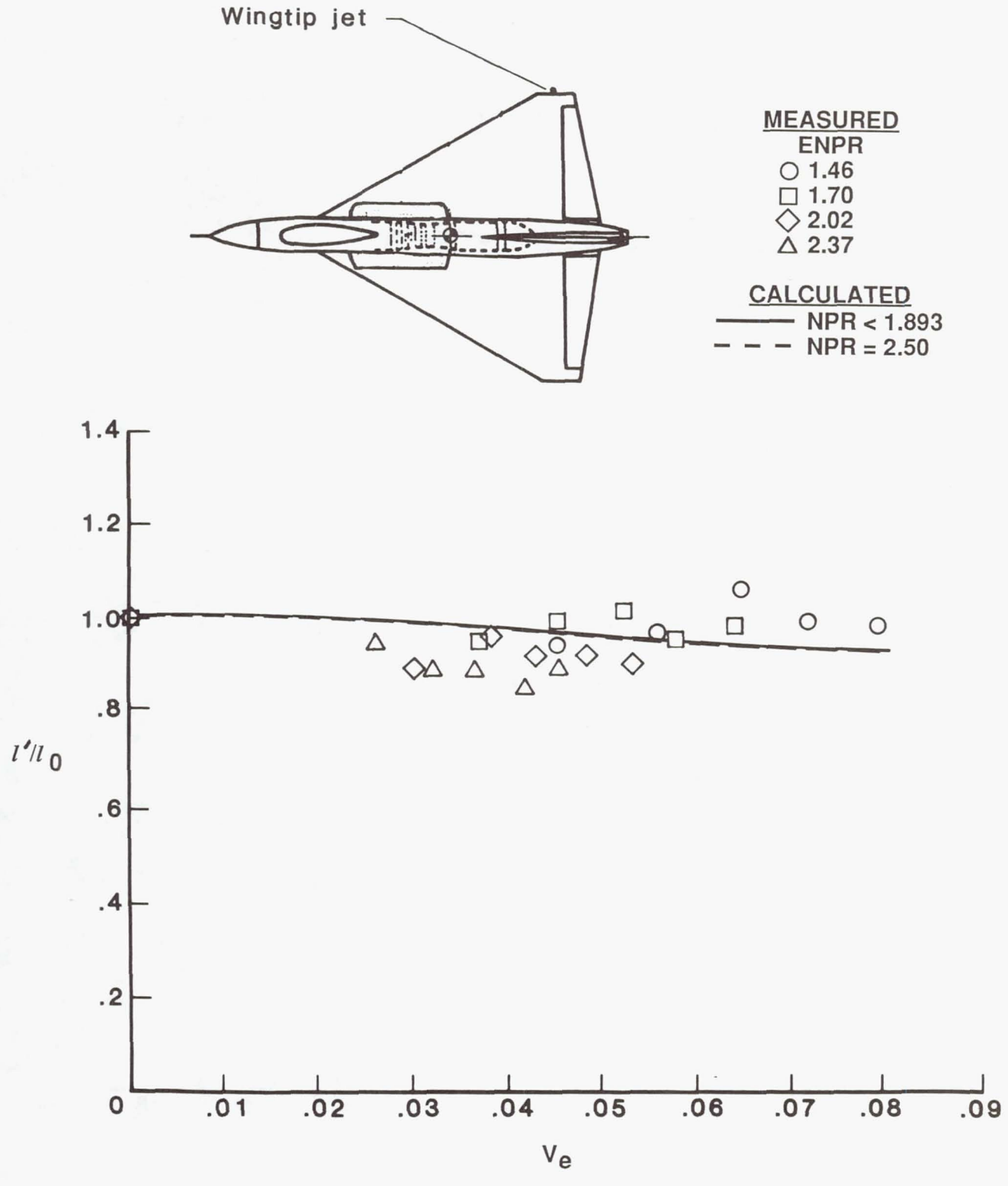

Figure 13. Effectiveness of wingtip roll jet for transition conditions. $\alpha = 0°$; $\beta = 0°$; $\delta_{e,L} = \delta_{e,R} = 0°$.

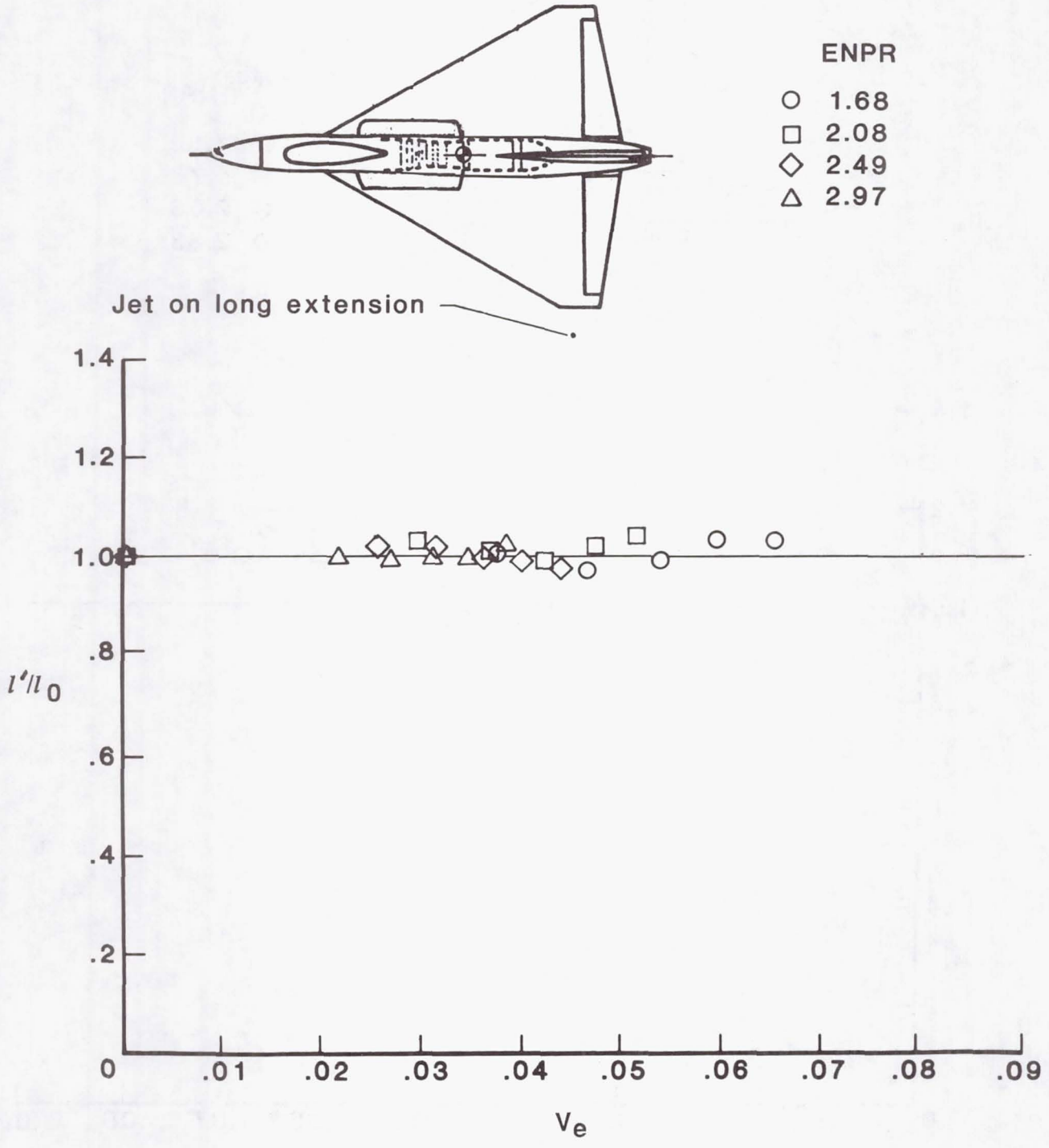

(a) Long extension on left wing.

Figure 14. Effectiveness of long-extended roll jets for transition conditions. $\alpha = 0°$; $\beta = 0°$; $\delta_{e,L} = \delta_{e,R} = 0°$; solid line indicates value at $l'/l_0 = 1.0$.

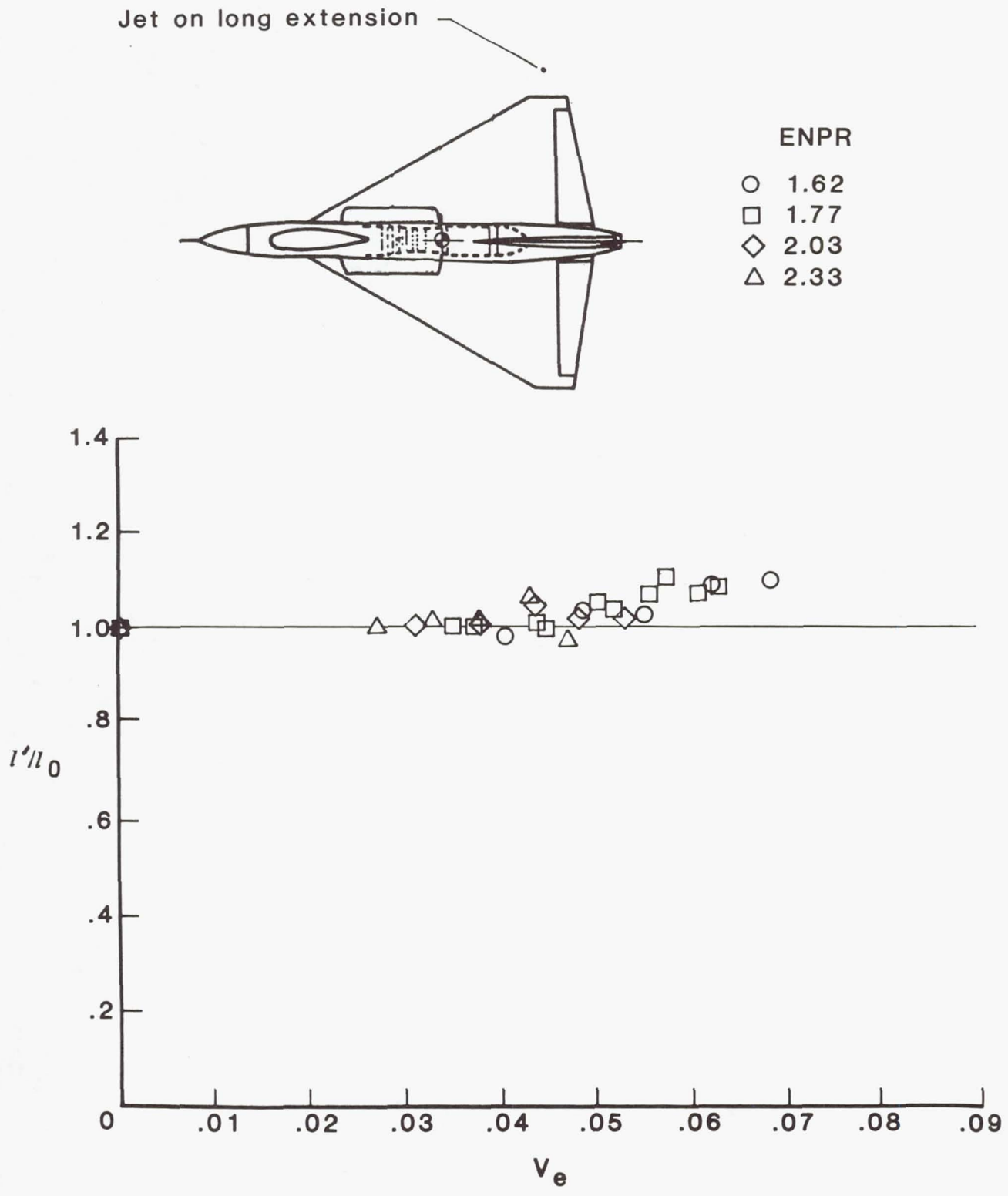

(b) Long extension on right wing.

Figure 14. Concluded.

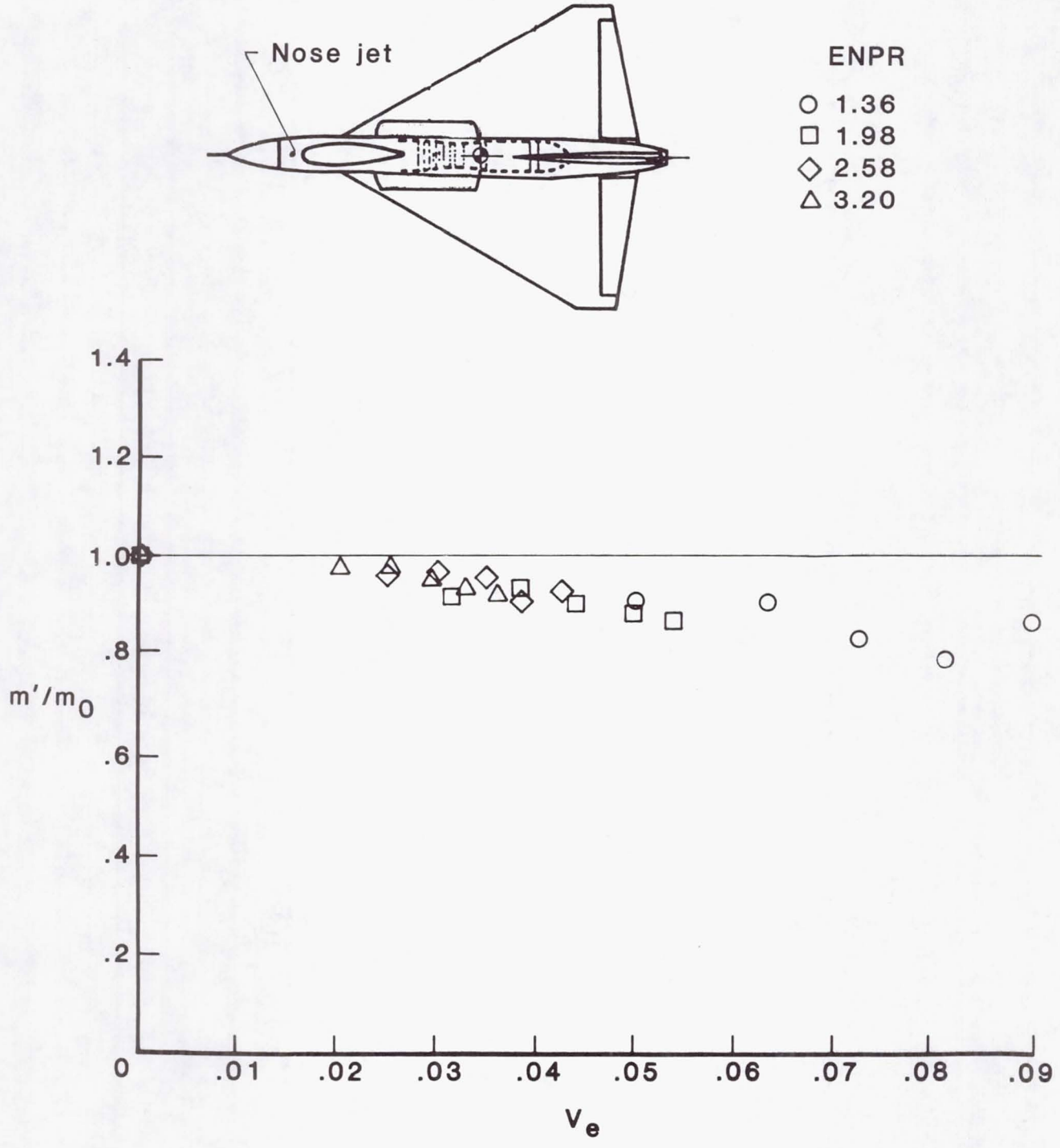

Figure 15. Effectiveness of nose jet for transition conditions. $\alpha = 0°$; $\beta = 0°$; $\delta_{e,L} = \delta_{e,R} = 0°$; solid line indicates value at $m'/m_0 = 1.0$.

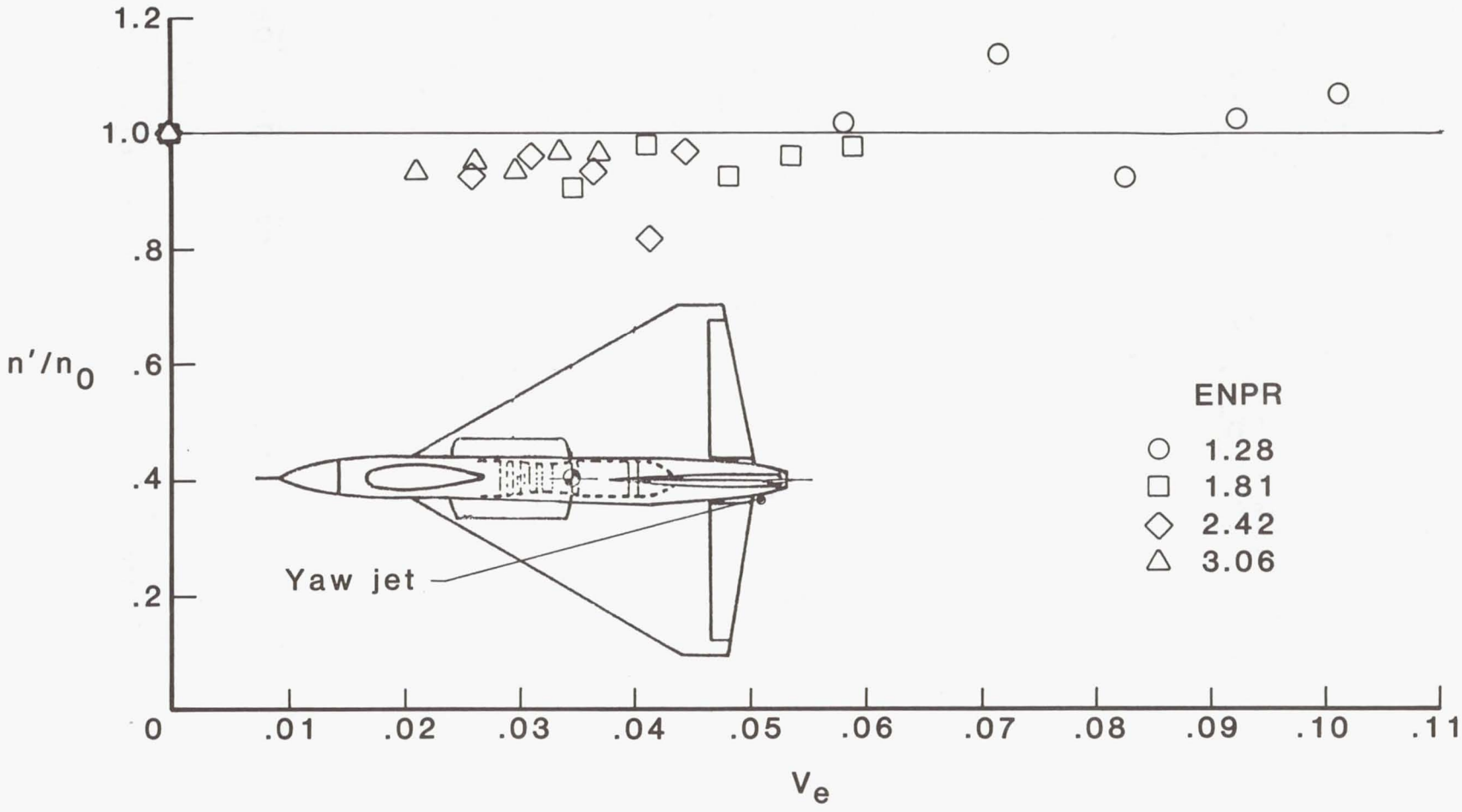

Figure 16. Effectiveness of left yaw jet for transition conditions. $\alpha = 0°$; $\beta = 0°$; $\delta_{e,L} = \delta_{e,R} = 0°$; solid line indicates value at $n'/n_0 = 1.0$.

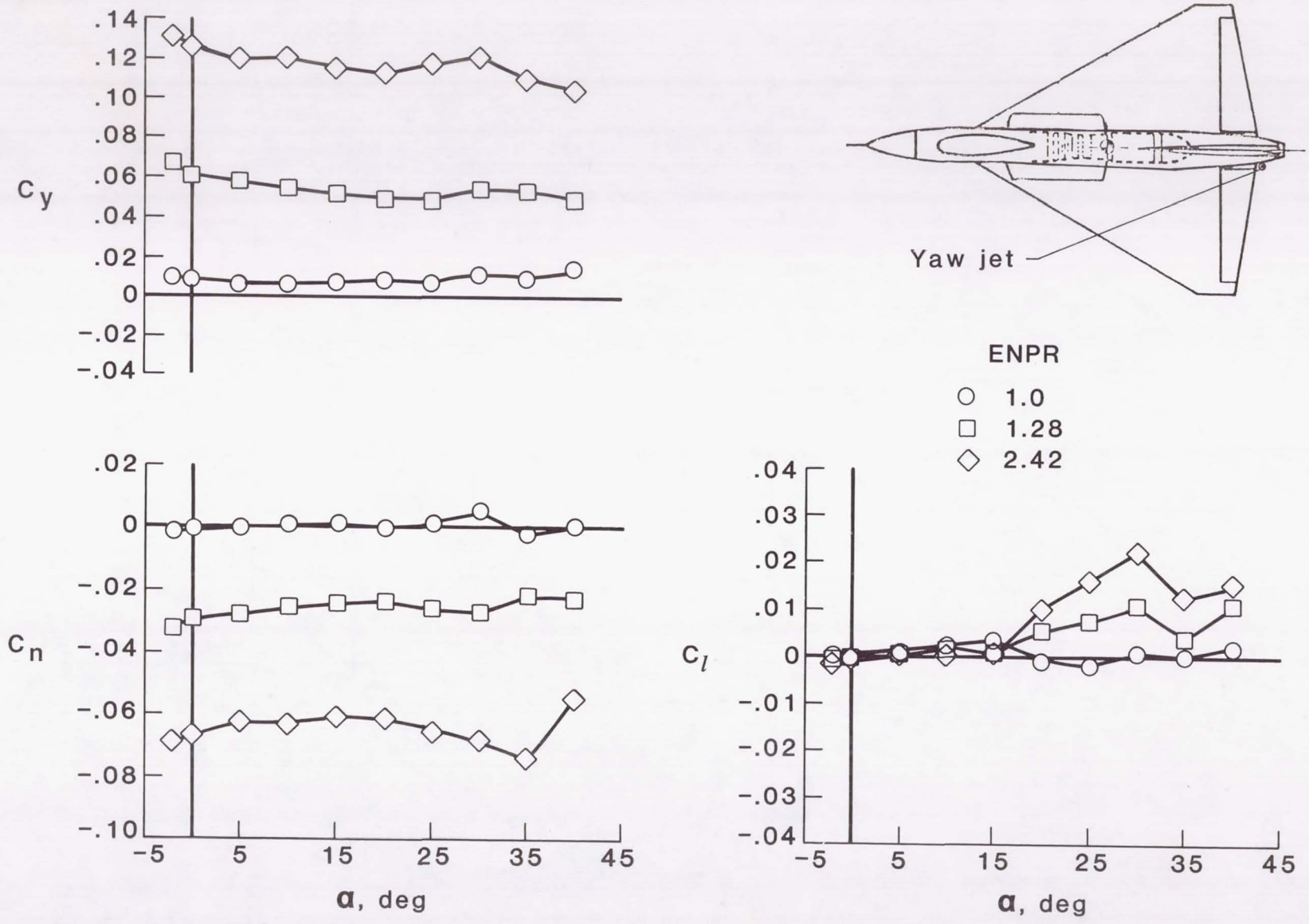

Figure 17. Lateral aerodynamic coefficients versus α for model with left yaw jet operating at several pressure settings. $\beta = 0°$; $q_\infty = 4$ lb/ft^2; $\delta_{e,L} = \delta_{e,R} = 0°$.

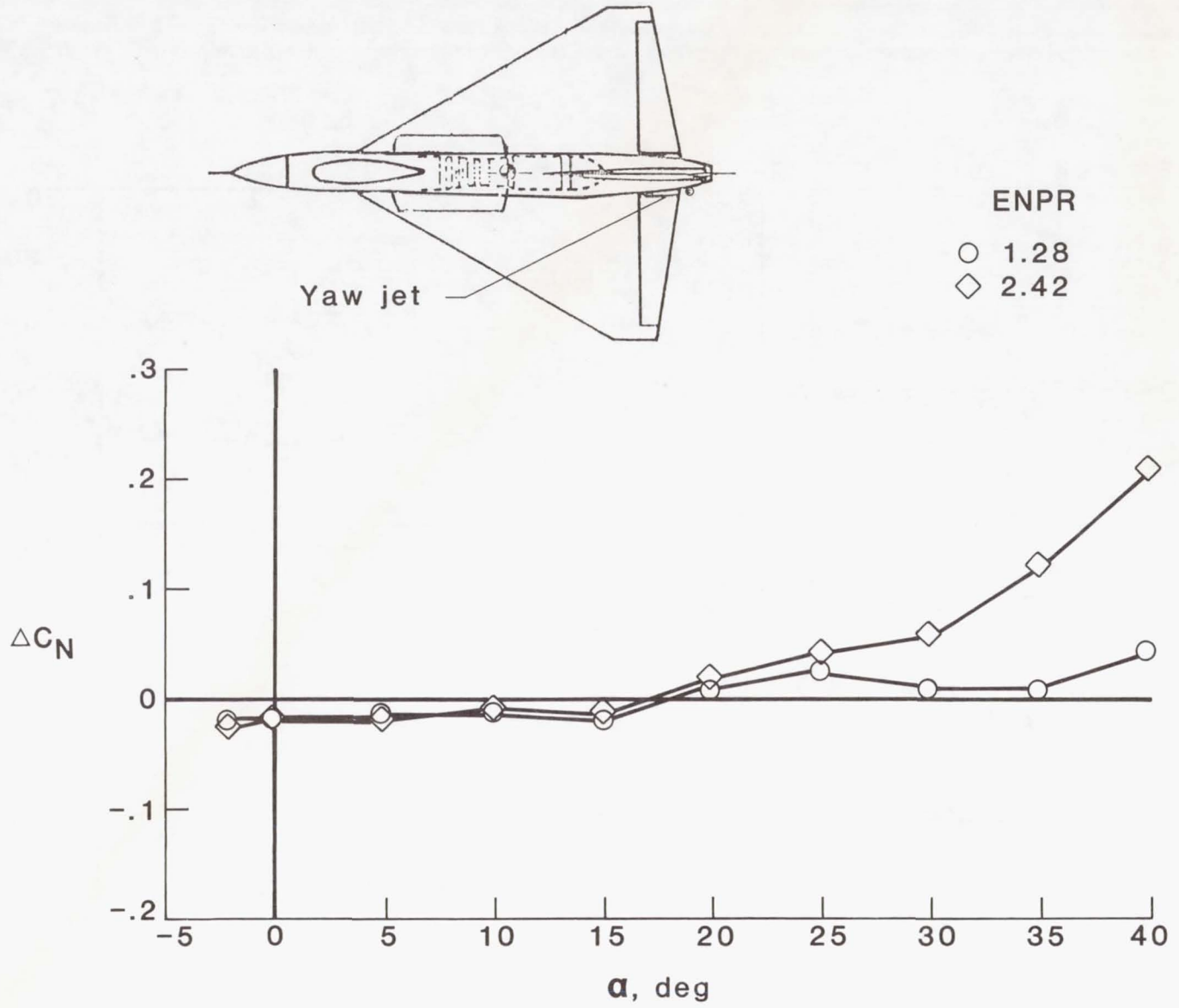

Figure 18. Jet-induced normal-force increments due to yaw jet operation. $\beta = 0°$; $q_\infty = 4$ lb/ft^2; $\delta_{e,L} = \delta_{e,R} = 0°$.

NASA
National Aeronautics and Space Administration

Report Documentation Page

1. Report No.	2. Government Accession No.	3. Recipient's Catalog No.
NASA TM-4147		

4. Title and Subtitle	5. Report Date
Low-Speed Wind-Tunnel Study of Reaction Control-Jet Effectiveness for Hover and Transition of a STOVL Fighter Concept	December 1989
	6. Performing Organization Code
7. Author(s)	8. Performing Organization Report No.
Donald R. Riley, Gautam H. Shah, and Richard E. Kuhn	L-16616
9. Performing Organization Name and Address	10. Work Unit No.
NASA Langley Research Center Hampton, VA 23665-5225	505-61-71-07
	11. Contract or Grant No.
12. Sponsoring Agency Name and Address	13. Type of Report and Period Covered
National Aeronautics and Space Administration Washington, DC 20546-0001	Technical Memorandum
	14. Sponsoring Agency Code

15. Supplementary Notes

Donald R. Riley and Gautam H. Shah: Langley Research Center, Hampton, Virginia.
Richard E. Kuhn: San Diego, California.

16. Abstract

A brief wind-tunnel study was conducted in the Langley 12-Foot Low-Speed Tunnel to determine reaction control-jet effectiveness and some associated aerodynamic characteristics of a 15-percent-scale model of the General Dynamics E-7A STOVL fighter concept applicable to hover and transition flight. Tests were made with the model at various attitude angles in the tunnel test section and at various tunnel airspeeds for a range of control-jet nozzle pressure ratios. Eight reaction control jets were tested individually. Four jets were at the design baseline locations providing roll, pitch, and yaw control. The remaining four jets were tested at alternate locations for roll control. Comparisons of measured data with values calculated using empirical methods were made where possible.

17. Key Words (Suggested by Authors(s))	18. Distribution Statement
VTOL STOVL Control jets Jets in crossflow	Unclassified—Unlimited Subject Category 08

19. Security Classif. (of this report)	20. Security Classif. (of this page)	21. No. of Pages	22. Price
Unclassified	Unclassified	37	A03

For sale by the National Technical Information Service, Springfield, Virginia 22161-2171